

MAY 17 1963
SCR-623



MASTER

Sandia Corporation

..... MONOGRAPH

TRANSIENT ELECTROMAGNETIC FIELD
PROPAGATION THROUGH INFINITE SHEETS,
INTO SPHERICAL SHELLS,
AND INTO HOLLOW CYLINDERS

by

C W Harrison, Jr

Facsimile Price \$ 5.60
Microfilm Price \$ 1.85

Available from the
Office of Technical Services
Department of Commerce
Washington 25, D. C.

APRIL 1963

DISCLAIMER

This report was prepared as an account of work sponsored by an agency of the United States Government. Neither the United States Government nor any agency Thereof, nor any of their employees, makes any warranty, express or implied, or assumes any legal liability or responsibility for the accuracy, completeness, or usefulness of any information, apparatus, product, or process disclosed, or represents that its use would not infringe privately owned rights. Reference herein to any specific commercial product, process, or service by trade name, trademark, manufacturer, or otherwise does not necessarily constitute or imply its endorsement, recommendation, or favoring by the United States Government or any agency thereof. The views and opinions of authors expressed herein do not necessarily state or reflect those of the United States Government or any agency thereof.

DISCLAIMER

Portions of this document may be illegible in electronic image products. Images are produced from the best available original document.

Published by
Sandia Corporation,
a prime contractor to the
United States Atomic Energy Commission

LEGAL NOTICE

This report was prepared as an account of Government sponsored work.
Neither the United States, nor the Commission, nor any person acting on behalf
of the Commission:

A. Makes any warranty or representation, expressed or implied, with re-
spect to the accuracy, completeness, or usefulness of the information contained
in this report, or that the use of any information, apparatus, method, or process
disclosed in this report may not infringe privately owned rights; or

B. Assumes any liabilities with respect to the use of, or for damages re-
sulting from the use of any information, apparatus, method, or process disclosed
in this report.

As used in the above, "person acting on behalf of the Commission" includes
any employee or contractor of the Commission, or employee of such contractor,
to the extent that such employee or contractor of the Commission, or employee of
such contractor prepares, disseminates, or provides access to, any information
pursuant to his employment or contract with the Commission, or his employment
with such contractor.

SANDIA CORPORATION MONOGRAPH

TRANSIENT ELECTROMAGNETIC FIELD PROPAGATION
THROUGH INFINITE SHEETS, INTO SPHERICAL SHELLS,
AND INTO HOLLOW CYLINDERS

by

C. W. Harrison, Jr.

April 1963

ACKNOWLEDGMENT

Mr. C. S. Williams made many contributions to this work. The problems discussed in the paper were programmed for the Sandia Laboratory CDC-1604 computer by Mr. E. A. Aronson. Mrs. Margaret Houston plotted the graphs; they were inked under the direction of Mr. C. A. Tucker. The author extends thanks to all who participated in the preparation of this article.

SUMMARY

Gaussian electromagnetic field pulses of several durations are propagated through infinite sheets, into the interior of hollow cylinders, and into the interior of spherical shells. The plates, spheres, and cylinders contain no slots. The time history of the propagated pulses is computed. Finally, the field is calculated in the interior of a cylinder of finite length when connected at its ends by wire to a generator delivering a current pulse of gaussian shape.

The dimensions of the cavities are assumed to be sufficiently small that resonances are not excited by the highest significant frequency contained in the shortest pulse considered.

The numerical study is restricted to thin-walled aluminum shields 1/32 inch, 1/16 inch, 1/8 inch, and 1/4 inch thick. The half-amplitude widths of the pulses employed lie in the range 14 μ s to 2400 μ s.

It is shown that gaussian pulse electric fields defined on the surface of the plates and cylinders are propagated with little diminution in amplitude. When the incident pulse undergoes reflection at the boundary surface as well as transmission through the metal wall, the total attenuation sustained by the field is great. Thin spherical shells form effective magnetic shields. The electric field is small in the interior of thin-walled cylinders carrying extremely large transient currents.

TABLE OF CONTENTS

Page

| | |
|---|----|
| SUMMARY | 2 |
| Introduction | 5 |
| The Impinging Gaussian Pulse | 5 |
| The Transfer Functions for Sheets, Spheres, and Cylinders | 6 |
| The Form of the Integrals to be Evaluated by a Computer | 10 |
| Discussion of Graphs | 11 |
| Concluding Remarks | 13 |
| APPENDIX I -- THE NECESSITY FOR KNOWING THE TIME DEPENDENCE EMPLOYED IN DERIVING THE TRANSFER FUNCTIONS | 15 |
| APPENDIX II -- NOTES ON THE MACHINE EVALUATION OF THE CYLINDER TRANSFER FUNCTION | 16 |
| REFERENCES | 55 |
| SUPPLEMENTAL REFERENCES | 55 |

LIST OF ILLUSTRATIONS

| | |
|---|----|
| Figure 1 -- Configurations Considered in the Propagation of Gaussian Pulses through Aluminum Walls | 19 |
| Graph 1 Input Gaussian Pulses | 20 |
| Graph 2 Infinite Plate, Steady-State Transfer Characteristic Relating E_i to E_t | 21 |
| Graph 3 Infinite Plate. $e_t(o) = 1 \text{ volt/m}$; $t_1 = 6 \mu\text{s}$ | 22 |
| Graph 4 Infinite Plate. $e_t(o) = 1 \text{ volt/m}$; $t_1 = 12 \mu\text{s}$ | 23 |
| Graph 5 Infinite Plate. $e_t(o) = 1 \text{ volt/m}$; $t_1 = 24 \mu\text{s}$ | 24 |
| Graph 6 Infinite Plate. $e_t(o) = 1 \text{ volt/m}$; $t_1 = 48 \mu\text{s}$ | 25 |
| Graph 7 Infinite Plate, Steady-State Transfer Characteristic Relating E_i to E_o | 26 |
| Graph 8 Infinite Plate. $e_o(o) = 1 \text{ volt/m}$; $t_1 = 6 \mu\text{s}$ | 27 |
| Graph 9 Infinite Plate. $e_o(o) = 1 \text{ volt/m}$; $t_1 = 12 \mu\text{s}$ | 28 |
| Graph 10 Infinite Plate. $e_o(o) = 1 \text{ volt/m}$; $t_1 = 24 \mu\text{s}$ | 29 |
| Graph 11 Infinite Plate. $e_o(o) = 1 \text{ volt/m}$; $t_1 = 48 \mu\text{s}$ | 30 |
| Graph 12 Sphere 36 Inches in Diameter. Steady-State Transfer Characteristic Relating H_i to H_o | 31 |
| Graph 13 Sphere 36 Inches in Diameter. $h_o(o) = 1 \text{ ampere/m}$; $t_1 = 24 \mu\text{s}$ | 32 |
| Graph 14 Sphere 36 Inches in Diameter. $h_o(o) = 1 \text{ ampere/m}$; $t_1 = 48 \mu\text{s}$ | 33 |
| Graph 15 Sphere 36 Inches in Diameter. $h_o(o) = 1 \text{ ampere/m}$; $t_1 = 96 \mu\text{s}$ | 34 |
| Graph 16 Sphere 36 Inches in Diameter. $h_o(o) = 1 \text{ ampere/m}$; $t_1 = 1000 \mu\text{s}$ | 35 |
| Graph 17 Sphere 72 Inches in Diameter. Steady-State Transfer Characteristic Relating H_i to H_o | 36 |
| Graph 18 Sphere 72 Inches in Diameter. $h_o(o) = 1 \text{ ampere/m}$; $t_1 = 24 \mu\text{s}$ | 37 |
| Graph 19 Sphere 72 Inches in Diameter. $h_o(o) = 1 \text{ ampere/m}$; $t_1 = 48 \mu\text{s}$ | 38 |
| Graph 20 Sphere 72 Inches in Diameter. $h_o(o) = 1 \text{ ampere/m}$; $t_1 = 96 \mu\text{s}$ | 39 |

LIST OF ILLUSTRATIONS (continued)

Page

| | | |
|----------|---|----|
| Graph 21 | Sphere 72 Inches in Diameter. $h_o(o) = 1$ ampere/m; $t_1 = 1000 \mu s$ | 40 |
| Graph 22 | Cylinder Steady-State Transfer Characteristic Relating E_i to E_t | 41 |
| Graph 23 | Cylinder. $e_t(o) = 1$ volt/m; $t_1 = 6 \mu s$ | 42 |
| Graph 24 | Cylinder. $e_t(o) = 1$ volt/m; $t_1 = 12 \mu s$ | 43 |
| Graph 25 | Cylinder. $e_t(o) = 1$ volt/m; $t_1 = 24 \mu s$ | 44 |
| Graph 26 | Cylinder. Steady-State Transfer Characteristic Relating E_i to E_o | 45 |
| Graph 27 | Cylinder. $e_o(o) = 1$ volt/m; $t_1 = 6 \mu s$ | 46 |
| Graph 28 | Cylinder. $e_o(o) = 1$ volt/m; $t_1 = 12 \mu s$ | 47 |
| Graph 29 | Cylinder. $e_o(o) = 1$ volt/m; $t_1 = 24 \mu s$ | 48 |
| Graph 30 | Cylinder. Steady-State Transfer Characteristic Relating E_i to I_o | 49 |
| Graph 31 | Cylinder. $i_o(o) = 1$ ampere; $t_1 = 12 \mu s$ | 50 |
| Graph 32 | Cylinder. $i_o(o) = 1$ ampere; $t_1 = 24 \mu s$ | 51 |
| Graph 33 | Cylinder. $i_o(o) = 1$ ampere; $t_1 = 48 \mu s$ | 52 |
| Graph 34 | Jupiter Missile. Steady-State Transfer Characteristic Relating E_i to I_o | 53 |
| Graph 35 | Jupiter Missile. $i_o(o) = 1$ ampere; $t_1 = 24, 48, \text{ and } 96 \mu s$ | 54 |

TRANSIENT ELECTROMAGNETIC FIELD PROPAGATION
THROUGH INFINITE SHEETS, INTO SPHERICAL SHELLS,
AND INTO HOLLOW CYLINDERS

Introduction

This study was undertaken to determine the shielding characteristics of thin-walled infinite sheets, spherical shells, and cylindrical tubes, illustrated by Figure 1, under transient conditions. The shields are made of aluminum and contain no slots. Gaussian electromagnetic field pulses are propagated through the infinite sheets, and from outside to the inside of closed containers in the geometrical shape of spheres and cylinders. Time histories of the attenuated pulses are computed. For the case of the infinite conductive sheets the propagated pulses are compared to the associated impinging pulses on the basis of available energy per unit area.

Finally, the field is calculated in the interior of cylindrical tubes of finite lengths, when the ends are connected by wire to a generator delivering a current pulse of gaussian shape. From the theoretical point of view, this problem is closely related to that of calculating the field within a missile stripped of interior components, when subjected to a direct lightning strike.

The Impinging Gaussian Pulse

The description of the impinging pulse in the time domain employed in this paper is

$$e(t) = A e^{-\frac{1}{2} \left(\frac{t}{t_1}\right)^2}, \quad (1)$$

where A is the value of $e(0)$, t is the time, and t_1 is a measure of the pulse width. The spectrum of the pulse is obtained by taking the Fourier transform of (1). Thus,

$$E(f) = A \int_{-\infty}^{\infty} e^{-\frac{1}{2} \left(\frac{t}{t_1}\right)^2} e^{-j2\pi f t} dt = A t_1 \sqrt{2\pi} e^{-\frac{1}{2} \left(\frac{f}{f_1}\right)^2} \quad (2)$$

where

$$f_1 = \frac{1}{2\pi t_1}. \quad (3)$$

In evaluating Fourier transforms by numerical methods it is often convenient to truncate the frequency spectrum in passing from the frequency to time domain, and truncate the limits of integration when computing the frequency spectrum of a given time function.

Let $e_1(t)$ be the new time function obtained by taking the transform of the truncated frequency function. Assume that the cutoff frequency is $f_c = 2.6f_1$. The error is then

$$\eta(t) = |e(t) - e_1(t)| = \left| \int_{-\infty}^{-2.6f_1} E(f) e^{j2\pi ft} df + \int_{2.6f_1}^{\infty} E(f) e^{j2\pi ft} df \right|. \quad (4)$$

Thus,

$$\eta(t) \leq 2 \int_{2.6f_1}^{\infty} |E(f)| df. \quad (5)$$

Substituting (2) into (5) and integrating, $\eta(t) \leq 0.0093A$. Thus, $e_1(t)$ does not depart from $e(t)$ by more than 1 percent at any time.

If $e(t)$ is a plane wave, the energy in the pulse is given by

$$U_t = \frac{1}{\zeta_0} \int_{-\infty}^{\infty} [e(t)]^2 dt = \frac{1}{\zeta_0} \int_{-\infty}^{\infty} |E(f)|^2 df, \quad (6)$$

where the last relation follows from Parseval's identity.

The energy lost by truncation of the spectrum is

$$U_f = \frac{2}{\zeta_0} \int_{2.6f_1}^{\infty} |E(f)|^2 df. \quad (7)$$

In these expressions $\zeta_0 = 120\pi$ ohms is the characteristic resistance of space. Substituting (2) into (6) and (7), and performing the integration, it is found that $U_f = 0.000236U_t$. Thus, 0.0236 of 1 percent of the energy is lost by truncation of the frequency spectrum at $f = 2.6f_1$.

In this paper the highest significant frequency contained in a gaussian pulse is taken to be $f_c = 2.6f_1 = 2.6/2\pi t_1$. The "significant" base width of the time function is $2 \times 2.6t_1 = 5.2t_1$. Thus, when $t_1 = 12 \mu s$ the pulse duration is considered to be $62.4 \mu s$. The highest significant frequency in this pulse is 34.48 kcs. The half-amplitude width of a gaussian pulse is $2.355t_1$.

The Transfer Functions for Sheets, Spheres, and Cylinders

It is readily shown from elementary principles of electrodynamics that the transfer functions for an infinite sheet of thickness d for parallel incidence of the electric field are^{1,2}

$$\frac{E_i(f)}{E_o(f)} = \frac{2\zeta_0\zeta}{2\zeta_0\zeta \cos kd + j(\zeta_0^2 + \zeta^2) \sin kd}, \quad (8)$$

and

$$\frac{E_i(f)}{E_t(f)} = \frac{\zeta_o}{\zeta_o \cos kd + j\zeta \sin kd}, \quad (9)$$

where $E_i(f)$ is the electric field emerging from the far side of the sheet, $E_o(f)$ is the incident electric field, and $E_t(f)$ is the tangential electric field on the near side of the sheet.* This field is the vector sum of the incident and reflected fields. $E_o(f) \gg E_i(f)$, and when $f > 0$, $E_t(f) > E_i(f)$ because of skin effect (refer to Figure 1).

$$\zeta = \sqrt{\frac{\pi f \mu}{\sigma}} (1 + j), \quad (10)$$

$$k = \sqrt{\pi f \mu \sigma} (1 - j), \quad (11)$$

where $\mu = 4\pi \times 10^{-7}$ henry/m is the permeability of space and $\sigma = 3.72 \times 10^7$ mhos/m is the conductivity of aluminum.

In deriving (8) and (9), a time dependence of the form $\exp(j2\pi ft)$ is assumed.

The transfer function for a spherical shell is

$$\frac{H_i(f)}{H_o(f)} = \frac{1}{\cosh \gamma d + \frac{1}{3} \gamma a \sinh \gamma d}. \quad (12)$$

Here, H_i is the magnetic field inside the spherical shell, H_o is the incident magnetic field, a is the outer radius of the shell, b is the inner radius of the shell, and $d = a - b$ is the shell thickness.

$$\gamma = \sqrt{\pi f \mu \sigma} (1 + j). \quad (13)$$

The cylinder transfer functions are⁴

$$\frac{E_i(f)}{E_t(f)} = \frac{J_o(kb)N_1(kb) - N_o(kb)J_1(kb)}{J_o(ka)N_1(kb) - N_o(ka)J_1(kb)}, \quad (14)$$

and

$$\frac{E_t(f)}{I_o(f)} = \frac{1}{\pi \sigma a^2} \left(\frac{ka}{2} \right) \cot kd. \quad (15)$$

In deriving (14) and (15), a time dependence of the form $\exp(j2\pi ft)$ is assumed. Here a and b are the outer and inner radii of the tube, respectively, and $d = a - b$ is the wall thickness.

* The subscripts i , o , and t on the fields mean inside, outside and tangential, respectively.

Now,⁵

$$J_o(kb)N_1(kb) - N_o(kb)J_1(kb) = -\frac{2}{\pi kb}. \quad (16)$$

(This is the Wronskian relation.) On combining (14) and (15), and making use of (16),

$$\frac{E_i(f)}{I_o(f)} = -\frac{\cot kd}{\pi \sigma ab} \left[\frac{1}{J_o(ka)N_1(kb) - N_o(ka)J_1(kb)} \right]. \quad (17)$$

This expression permits calculation of the steady-state field within the cylinder in terms of the total current delivered by the current generator directly connected by wire to the ends of the cylinder. It is assumed that the current is uniform in this circuit. This will be the case if the circuit dimensions are small in terms of the wavelength of the highest significant frequency contained in the shortest current pulse employed in this study.

If a plane-wave electric field is directed parallel to the axis of an isolated cylinder, the current $I_o(f)$ at its mid-point is obtained from antenna theory. It is given by the relation

$$I_o(f) = \frac{2h_e(f)E_o}{Z_o(f)}. \quad (18)$$

The effective length of the cylinder is $2h_e$, and Z_o is its impedance. If $\Omega \geq 7$ and $\beta h = \frac{2\pi}{\lambda} h \leq \frac{2\pi f_c}{c} h \leq 0.5$,⁶

$$2h_e(f) = \frac{\Omega(\Omega - 1)}{\Omega - 2 + \ln 4}, \quad (19)$$

and

$$Z_o(f) = \frac{\zeta_o}{6\pi}(\beta h)^2 \left[\frac{1 + \frac{4 \ln 2}{\Omega - 2}}{\left(1 + \frac{2 \ln 2}{\Omega - 2}\right)^2} \right] - j \frac{\zeta_o}{2\pi\beta h} \left[\frac{\Omega - 2}{1 + \frac{2 \ln 2}{\Omega - 2}} \right], \quad (20)$$

where Ω is the cylinder shape parameter. It is

$$\Omega = 2 \ln \frac{2h}{a}. \quad (21)$$

The length of the cylinder is $2h$.

It is of interest to note that as $f \rightarrow 0$, the transfer functions (8), (9), (12), (14), and (15) become

$$\left. \frac{E_i(0)}{E_o(0)} \right|_{\text{plate}} = \frac{1}{1 + \frac{\zeta_o \sigma d}{2}}, \quad (22a)$$

$$\left. \frac{E_i(0)}{E_t(0)} \right|_{\text{plate}} = 1, \quad (22b)$$

$$\left. \frac{H_i(o)}{H_o(o)} \right|_{\text{sphere}} = 1, \quad (22c)$$

$$\left. \frac{E_i(o)}{E_t(o)} \right|_{\text{cylinder}} = 1, \quad (22d)$$

$$\left. \frac{E_t(o)}{I_o(o)} \right|_{\text{cylinder}} = \frac{1}{2\pi\sigma ad}. \quad (22e)$$

Also, from (18) as $f \rightarrow o$,

$$I_o(o) \left|_{\text{antenna}} \right. = 0. \quad (22f)$$

Let

$$G(f) = G_R(f) + jG_I(f) \quad (23)$$

represent any one of the foregoing transfer functions. It can be readily verified by expanding the trigonometric, hyperbolic, and Bessel functions in series, and examining the resulting expressions, that they satisfy the relation

$$G^*(f) = G(-f). \quad (24)$$

That this holds for (18) follows from the fact that $Z_o^*(f) = Z_o(-f)$, as an inspection of (20) shows. Expression (24) sets forth an important property of any transfer function applying to a physically realizable system.

From (23)

$$G(-f) = G_R(-f) + jG_I(-f), \quad (25)$$

and by definition

$$G^*(f) = G_R(f) - jG_I(f). \quad (26)$$

It follows that

$$G_R(f) = G_R(-f) \quad (27)$$

is an even function, and

$$G_I(f) = -G_I(-f) \quad (28)$$

is an odd function.

The Form of the Integrals to be Evaluated by a Computer

For illustrative purposes, let it be supposed that the time function of the electric field within a hollow cylinder is to be computed in terms of the gaussian pulse current the generator delivers by wire to the ends of the cylinder. In this instance, $G(f)$ is the shorthand notation for the right-hand side of (17). Then,

$$E_i(f) = G(f) I_o(f). \quad (29)$$

$I_o(f)$ corresponds to (2), that is,

$$I_o(f) = At_1 \sqrt{2\pi} e^{-\frac{1}{2} \left(\frac{f}{f_1}\right)^2} \quad (30)$$

for a current pulse in the time domain corresponding to (1). A is in amperes, and $I_o(f)$ in amperes/Hz for this particular situation.

The time history of the field on the interior of the cylinder is available from the integral

$$e_i(t) = At_1 \sqrt{2\pi} \int_{-\infty}^{\infty} G(f) e^{-\frac{1}{2} \left(\frac{f}{f_1}\right)^2} e^{j2\pi ft} df$$

$$\sim At_1 \sqrt{2\pi} \int_{-f_c}^{f_c} \left\{ G_R(f) \cos 2\pi ft - G_I(f) \sin 2\pi ft \right. \\ \left. + j [G_R(f) \sin 2\pi ft + G_I(f) \cos 2\pi ft] \right\} e^{-\frac{1}{2} \left(\frac{f}{f_1}\right)^2} df, \quad (31)$$

provided the time dependence assumed in deriving $G(f)$ is $\exp(j2\pi ft)$. Since $G_R(f)$ and $\cos 2\pi ft$ are even functions, and $G_I(f)$ and $\sin 2\pi ft$ are odd functions, it follows that (32) reduces to

$$e_i(t) = 2At_1 \sqrt{2\pi} \int_0^{f_c} [G_R(f) \cos 2\pi ft - G_I(f) \sin 2\pi ft] e^{-\frac{1}{2} \left(\frac{f}{f_1}\right)^2} df. \quad (32)$$

This is the final form of the integral to be evaluated on the computer. Note that the integral is necessarily real because $e_i(t)$ is a real function of time. All of the integrals encountered in this paper concerning the various shields are similar in form to (32). The constant A was taken as unity throughout the work. Of course, the units of A will depend on the shielding problem being considered.

Discussion of Graphs

Graph 1 shows the amplitude-time relation of some of the input gaussian pulses used in the numerical study. Specifically, pulses are drawn for values t_1 of 6, 12, 24, and 48 μ s. Note that the peak amplitude of unity occurs at zero time. The pulses are symmetrical on the time scale.

Graph 2, based on (9), gives the steady-state transfer characteristic relating $E_i(f)$ to $E_t(f)$ for an infinite aluminum plate of thickness 1/32 inch, 1/16 inch, and 1/8 inch. For example, for a 1/16-inch plate at 15 kcs, the field emerging from the plate $E_i(f)$ is 30 db below the tangential field $E_t(f)$ on the other side of the plate.

Graphs 3, 4, 5, and 6 give the time history of the field $e_i(t)$ emerging from the plates of designated thicknesses in terms of $e_t(t)$ for values of t_1 of 6, 12, 24, and 48 μ s, respectively. The value of $e_t(0)$ is 1 volt/m. Note that in all cases, the attenuation of the field is not great, but progressively increases with plate thickness and decreasing values of t_1 . The waves are retarded in time in propagating through the plates, as should be anticipated. The delay increases with plate thickness.

Graph 7, based on (8), is like Graph 2, except that $e_o(t)$ replaces $e_t(t)$.

Graphs 8, 9, 10, and 11 correspond to Graphs 3, 4, 5, and 6, respectively, except that $e_o(t)$ replaces $e_t(t)$. Note that the wave shapes are very much alike, but the amplitude scale is vastly different. Graph 8 shows, for example, that when the peak value of $e_o(t)$ is 1 volt/m, $t_1 = 6 \mu$ s, and $d = 1/32$ inch the peak value of $e_i(t)$ is about 1.61×10^{-7} volts/m, and occurs at 0.01 ms. If $e_o(t) = 10^5$ volts/m, $e_i(t) = 0.0161$ volts/m. Note that $e_o(t)$ undergoes reflection at the boundary surface, and this accounts for the large attenuation afforded by the sheet.

Graph 12, based on (12), gives the steady-state transfer characteristic relating $H_i(f)$ to $H_o(f)$ for a 36-inch spherical shell made of aluminum having wall thicknesses of 1/32 inch, 1/16 inch, and 1/8 inch. As an illustration, for a 1/16-inch wall 36-inch sphere at 7 kcs, the magnetic field $H_i(f)$ on the interior of the sphere is 56 db below the incident magnetic field $H_o(f)$.

Graphs 13, 14, 15, and 16 give the time history of the magnetic field $h_i(t)$ inside the 36-inch spheres of designated wall thicknesses when the magnetic field $h_o(0) = 1$ ampere/m for t_1 values of 24, 48, 96, and 1000 μ s, respectively. As expected, as the pulse length increases, the field $h_i(t)$ increases. The thicker the shield, the more effective it becomes. Note the severe distortion of the incident pulse in propagating into the interior of the sphere.

Graph 17 is like Graph 12, except that it applies to a 72-inch spherical shell.

Graphs 18, 19, 20, and 21 correspond to Graphs 13, 14, 15, and 16, respectively, except that the computations were carried out for a 72-inch spherical shell.

Graph 22, based on (14), gives the steady-state transfer characteristic relating $E_i(f)$ to $E_t(f)$ for a cylinder 22.08 feet in length and 16 inches in diameter when the wall thicknesses are 1/32 inch, 1/16 inch, and 1/8 inch.

Graphs 23, 24, and 25 give the time history of the field $e_i(t)$ in the interior of the above cylinder when $e_i(0) = 1$ volt/m for t_1 values of 6, 12, and 24 μ s. These graphs applying to finite cylinders have much in common with Graphs 3, 4, and 5 applying to infinite plates.

Graph 26, computed from (14), (15), and (18), permits one to obtain the db ratio of $E_i(f)$ to $E_o(f)$ under steady-state conditions for a cylinder 22.08 feet in length and 16 inches in diameter, when the plate thickness and frequency are specified.

Graphs 27, 28, and 29 furnish the time history of $e_i(t)$ for $e_o(0)$ of 1 volt/m for the designated cylinder for t_1 values of 6, 12, and 24 μ s and for wall thicknesses of 1/32 inch, 1/16 inch, and 1/8 inch. Note that the interior field is extremely minute in terms of the incident field. Most of this attenuation is due to the fact that the incident field is reflected by the cylinder; the field $e_i(t)$ is extremely small compared to $e_o(t)$. Observe that the field on the interior of the cylinder is oscillatory in nature. This is accounted for by the fact that the transfer characteristic $E_i(f)/E_o(f)$, obtained by eliminating $I_o(f)$ between (17) and (18) rises with increasing frequency, and then falls off as the frequency is still further increased, as Graph 26 shows. No other transfer functions employed in this paper exhibit this property. The phenomenon is not to be attributed to antenna resonance. The cylinder remains short in terms of the wavelength of the highest significant frequency contained in the shortest pulse considered in the analysis.

Graph 30, computed from (17), furnishes the ratio of $E_i(f)/I_o(f)$ as a function of frequency for a cylinder 22.08 feet in length and 16 inches in diameter having wall thicknesses of 1/32 inch, 1/16 inch, and 1/8 inch. Thus, for a total current in any cross section of the cylinder of 1 ampere, the field in the interior of the cylinder will be 10^{-10} volts/m, if the frequency is 150 kcs and the cylinder wall thickness is 1/8 inch.

Graphs 31, 32, and 33 give the time history of $e_i(t)$, when $i_o(0)$ is 1 ampere, for the cylinders mentioned above for t_1 values of 12, 24, and 48 μ s.

Graph 34 is the same as Graph 30, but is computed for a cylinder 105 inches in diameter, 60 feet 4 inches in height, and having a wall thickness of 1/4 inch. These dimensions are reported to apply to a Jupiter missile.

Graph 35 presents the time history of the electric field $e_i(t)$ inside a Jupiter missile stripped of interior components when $i_o(0)$ is 1 ampere for t_1 values of 24, 48, and 96 μ s. Observe that the height dimension of the missile is sufficiently small that the current is uniform in the circuit connecting the ends of the missile to the current pulse generator.

Table I presents the decibel ratio of the energy available in the emerging plane-wave pulse from the far side of the plate to the energy in the impinging plane-wave pulse on the near side of the plate for the cases of tangential and incident electric fields. The decibel ratio of the propagated and impinging pulse peaks in the various situations described in the paper is easily obtained by inspection, hence tables are not provided.

TABLE I
Decibel Ratio of Energy Available in the Emerging Plane-Wave Pulse
from the Far Side of a Plate to the Energy in the
Impinging Plane-Wave Pulse on the Near Side of the Plate

| (a) | | | (b) | | |
|--|------------|-----|--|------------|------|
| Case of the tangential electric field | | db | Case of the incident electric field | | db |
| d | t_1 | db | d | t_1 | db |
| 1/32 inch | 6 μ s | - 4 | 1/32 inch | 6 μ s | -138 |
| 1/16 inch | 6 μ s | - 6 | 1/16 inch | 6 μ s | -147 |
| 1/8 inch | 6 μ s | -11 | 1/8 inch | 6 μ s | -158 |
| 1/32 inch | 12 μ s | - 3 | 1/32 inch | 12 μ s | -138 |
| 1/16 inch | 12 μ s | - 5 | 1/16 inch | 12 μ s | -145 |
| 1/8 inch | 12 μ s | - 9 | 1/8 inch | 12 μ s | -155 |
| 1/32 inch | 24 μ s | - 3 | 1/32 inch | 24 μ s | -138 |
| 1/16 inch | 24 μ s | - 4 | 1/16 inch | 24 μ s | -144 |
| 1/8 inch | 24 μ s | - 6 | 1/8 inch | 24 μ s | -153 |
| 1/32 inch | 48 μ s | - 3 | 1/32 inch | 48 μ s | -138 |
| 1/16 inch | 48 μ s | - 4 | 1/16 inch | 48 μ s | -144 |
| 1/8 inch | 48 μ s | - 5 | 1/8 inch | 48 μ s | -151 |

Table I was computed from the relation

$$db = 10 \log_{10} \left\{ \frac{\int_{-\infty}^{\infty} [e_i(t)]^2 dt}{\int_{-\infty}^{\infty} [e_o(t)]^2 dt} \right\} = 10 \log_{10} \left\{ \frac{\int_{-\infty}^{\infty} [e_i(t)]^2 dt}{t_1 \sqrt{\pi}} \right\}. \quad (33)$$

Concluding Remarks

The shielding action of aluminum plates, spherical shells, and hollow cylinders to transient impinging fields and currents has been investigated rigorously. It has been assumed that the forcing pulses contain no frequencies sufficiently high to excite resonances in the spherical shells or hollow cylinders. The lowest mode of a perfectly conducting spherical shell is $\lambda_o = 2.28b$, where b is the inner radius. The lowest radial mode for a perfectly conducting cylinder, when the exciting electric field is parallel to the axis of the cylinder, is $\lambda_o = 2.61b$, where, again, b is the inner radius. The lowest longitudinal mode for the cylinder occurs when $2h \approx \lambda/2$. A moment's investigation will reveal that all of the cavity shields studied in this report have dimensions sufficiently small that no resonances can be excited by a frequency $f_c = 68.96$ kcs, which corresponds to $t_1 = 6 \mu$ s. This is the smallest value of t_1 of any gaussian pulse considered in the present analysis.

It should be evident to the reader that the use of gaussian pulses is not dictated by any theoretical considerations. Suppose $e_o(t)$ corresponding to a lightning flash is measured. Then, $E_o(f)$, the forcing function, can be found by numerical integration, by using a truncated form of the Fourier integral

$$E_o(f) = \int_{-\infty}^{\infty} e_o(t) e^{-j2\pi ft} dt,$$

for passing from the time to the frequency domain.

Having found the frequency spectrum $E_o(f)$ corresponding to the time function $e_o(t)$, one can find $e_i(t)$ numerically by using a truncated form of the Fourier integral

$$e_i(t) = \int_{-\infty}^{\infty} G(f) E_o(f) e^{j2\pi ft} df.$$

Thus, $e_i(t)$ can be found for any arbitrary wave shape $e_o(t)$ -- just as easily as was done for gaussian impinging pulses used in this report.

Center-loaded electric dipoles may be placed axially in the cylinders, and impedance-loaded loops in the spherical shells, and the energy in the loads evaluated under transient conditions. Consideration of these interesting problems is reserved for another paper.

APPENDIX I

THE NECESSITY FOR KNOWING THE TIME DEPENDENCE EMPLOYED IN DERIVING THE TRANSFER FUNCTIONS

It has been stressed that the time dependence employed in deriving the transfer functions given in this paper for sheets, spheres, and cylinders is $\exp(j2\pi ft)$. If the time dependence $\exp(-j2\pi ft)$ -- favored by many electrodynamists -- had been assumed in the development of (12), for example, the effect would have been to substitute k for γ . The transfer function then becomes $G^*(f)$ instead of $G(f) = H_1(f)/H_0(f)$. To obtain meaningful results in the solution of transient problems this change must be reflected by appropriate sign changes in the exponents of the Fourier transforms for passing from the frequency to the time domain, and vice versa.

Consider a series RL circuit (assumed to be linear). The driving voltage is $e(t)$ and the current in the circuit is $i(t)$. The differential equation is

$$c(t) = L \frac{di(t)}{dt} + Ri(t).$$

Let $e(t) = e^{j2\pi ft}$. Then, $i(t) = G(f)e^{j2\pi ft}$ where $G(f) = 1/(R + j\omega L)$. Construct the following table.

| Input | Output | |
|--|--|--|
| $e(t)$ | $i(t)$ | |
| $e^{j2\pi ft}$ | $G(f)e^{j2\pi ft}$ | |
| $E(f)e^{j2\pi ft}df$ | $E(f)G(f)e^{j2\pi ft}df$ | (Property of linear systems - multiply by $E(f)df$) |
| $\int_{-\infty}^{\infty} E(f)e^{j2\pi ft}df$ | $\int_{-\infty}^{\infty} E(f)G(f)e^{j2\pi ft}df$ | (Property of linear systems - integrate) |

Since $e(t) = \int_{-\infty}^{\infty} E(f)e^{j2\pi ft}df$, for consistency, $E(f) = \int_{-\infty}^{\infty} e(t)e^{-j2\pi ft}dt$.

Alternatively, if $e(t) = e^{-j2\pi ft}$ it follows that $G(f) = 1/(R - j\omega L)$,

$$i(t) = \int_{-\infty}^{\infty} E(f)G(f)e^{-j2\pi ft}df; e(t) = \int_{-\infty}^{\infty} E(f)e^{-j2\pi ft}df, \text{ and } E(f) = \int_{-\infty}^{\infty} e(t)e^{j2\pi ft}dt.$$

APPENDIX II

NOTES ON THE MACHINE EVALUATION OF THE CYLINDER TRANSFER FUNCTION

Let

$$G(z_1, z_2) = \frac{J_o(z_1)N_1(z_1) - N_o(z_1)J_1(z_1)}{J_o(z_2)N_1(z_1) - N_o(z_2)J_1(z_1)} = \frac{M}{D},$$

where $z_i = z_{iR} - jz_{iI}$, $Z_{iR} = Z_{iI}$, $i = 1, 2$. Also define $z_2 = z_1 + \delta$ (δ small)

- a. As mentioned in the body of the paper, as $f \rightarrow 0$, $G(0, 0) = 1 + jo$,
- b. When $0 < R_e(z_1) \leq 5$, $G(z_1, z_2)$ may be evaluated directly using single-precision arithmetic (36 bits); however, when $5 < R_e(z_1)$, $G(z_1, z_2)$ cannot be accurately evaluated directly using single-precision arithmetic because of loss of significant digits in the subtractions. In lieu of the extreme difficulties encountered in evaluating $G(z_1, z_2)$ with multiple-precision arithmetic, the following approximation was used.

Let

$$G(z_1, z_2) = \frac{M}{D} = \frac{M}{M + D - M},$$

where

$$D - M = N_1(z_1) \{J_o(z_2) - J_o(z_1)\} - J_1(z_1) \{N_o(z_2) - N_o(z_1)\}.$$

It is now possible to expand $J_o(z)$ and $N_o(z)$ in a Taylor series about z_1 . Recalling that $z_2 = z_1 + \delta$,

$$J_o(z_1 + \delta) - J_o(z_1) = \delta J'_o(z_1) + \frac{\delta^2}{2!} J''_o(z_1) + \frac{\delta^3}{3!} J'''_o(z_1) + \dots$$

A similar expansion holds for $N_o(z_1 + \delta) - N_o(z_1)$. Combining powers of δ , and realizing that all Bessel functions now have z_1 for their argument, yields

$$D - M = \delta \{N_1 J'_o - J_1 N'_o\} + \frac{\delta^2}{2!} \{N_1 J''_o - J_1 N''_o\} + \dots = \sum_{n=1}^{\infty} \frac{C_n \delta^n}{n!};$$

when $C_n = N_1 J_o^{(n)} - J_1 N_o^{(n)}$. It remains to evaluate C_n .

By virtue of the relationships $J'_o = -J_1$ and $N'_o = -N_1$, it follows that $C_1 = 0$.

Since J_o and N_o satisfy Bessel's equation,

$$J''_o(z) = -\frac{J'_o(z)}{z} - J_o(z),$$

and

$$N''_o(z) = -\frac{N'_o(z)}{z} - N_o(z),$$

$$C_2 = N_1 \left\{ -\frac{J'_o}{z} - J_o \right\} - J_1 \left\{ -\frac{N'_o}{z} - N_o \right\} = -N_1 J_o + J_1 N_o = -M.$$

Differentiating $J''(z)$ and $N''(z)$ yields

$$J''_o(z) = -\frac{J''_o(z)}{z} + \frac{J'_o(z)}{z^2} - J'_o(z),$$

$$N''_o(z) = -\frac{N''_o(z)}{z} + \frac{N'_o(z)}{z^2} - N'_o(z).$$

As before, the terms involving J'_o and N'_o cancel and

$$C_3 = \frac{M}{z} \Big|_{z=z_1} = \frac{M}{z_1}.$$

Differentiating again yields

$$J''''_o = -\frac{J''_o}{z} + 2\frac{J''_o}{z^2} - 2\frac{J'_o}{z^3} - J''_o$$

a similar expression holds for N''''_o . Now,

$$C_4 = C_2 \left[\frac{2}{z_1^2} - 1 \right] - \frac{C_3}{z_1} = -M \left[\frac{2}{z_1^2} - 1 \right] - \frac{M}{z_1^2} = M \left[1 - \frac{3}{z_1^2} \right].$$

It was decided that four terms of the expansion would be satisfactory for better than 1-percent accuracy in the range

$$5 < R_e(z_1) \leq 20.$$

One may now write

$$G(z_1, z_2) = \frac{M}{M + D - M} \approx \frac{M}{M - \frac{\delta^2}{2!} M + \frac{\delta^3}{3! z_1} M + \frac{\delta^4}{4!} \left[1 - \frac{3}{z_1^2} \right] M}$$

$$= \frac{1}{1 - \frac{\delta^2}{2!} + \frac{\delta^3}{3! z_1} + \frac{\delta^4}{4!} \left[1 - \frac{3}{z_1^2} \right]}.$$

This approximation was used for $5 < R_e(z_1) \leq 20$.

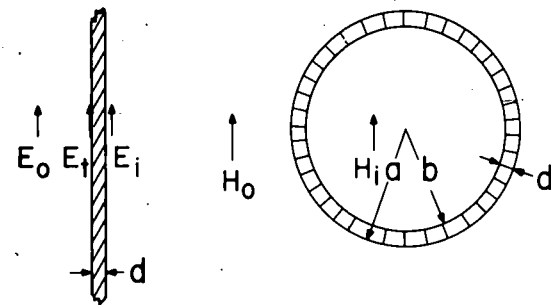
c. For $R_e(z_1) > 20$, two terms of the asymptotic expansion may be used.

We have,

$$M \cong -\frac{2}{\pi z_1},$$

$$D \cong -\frac{2}{\pi \sqrt{z_1 z_2}} \left\{ \cos \delta \left[1 - \frac{3}{64 z_1 z_2} \right] + \frac{\sin \delta}{8} \left[\frac{1}{z_2} + \frac{3}{z_1} \right] \right\},$$

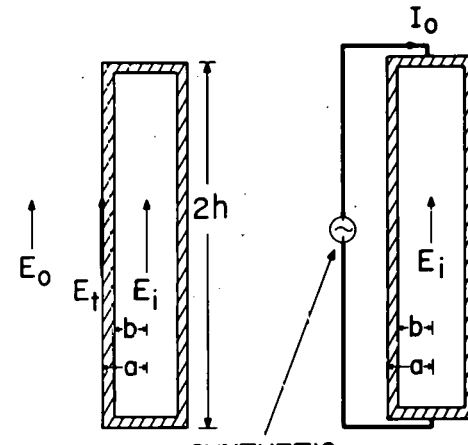
DIRECTION OF WAVE PROPAGATION



(a) INFINITE PLATE

(b) SPHERE

$$\lambda_o = 2.28b$$



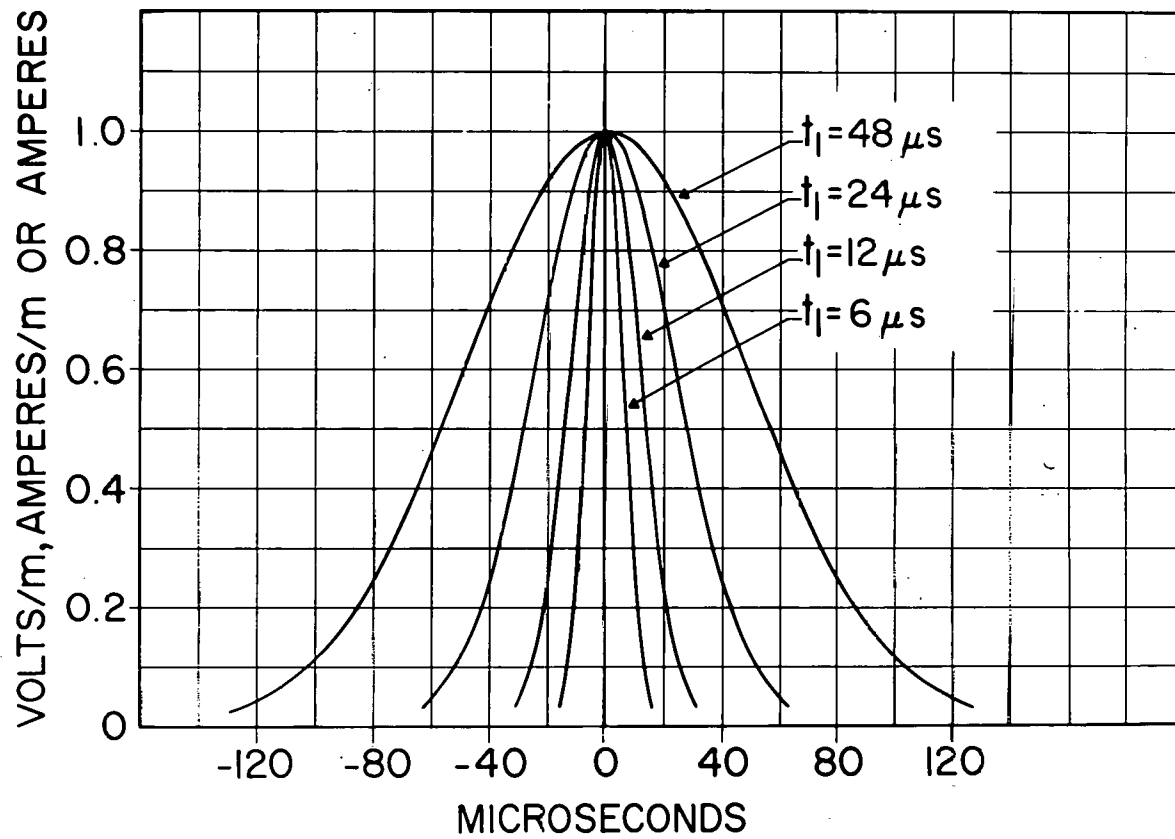
(c) CYLINDER

$$\lambda_o = 2.61b$$

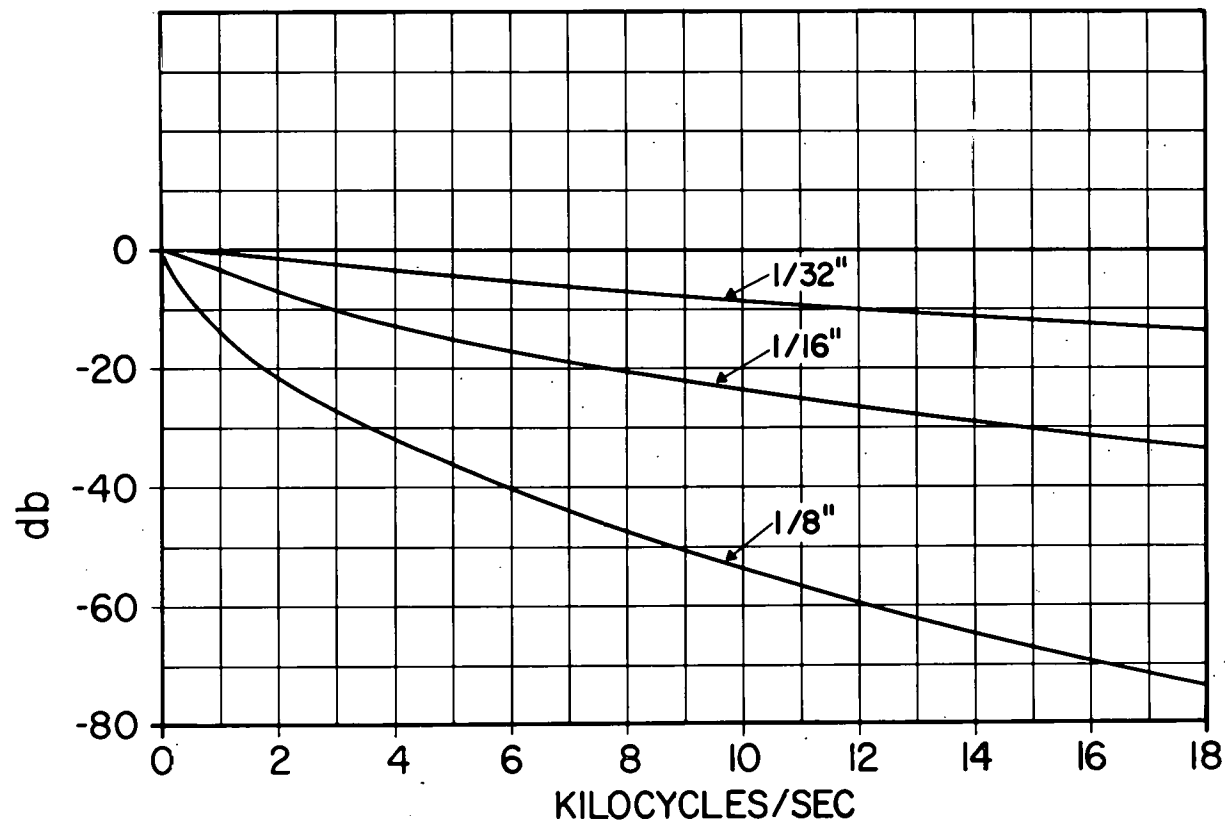
(d) CYLINDER WITH
DIRECT GENERATOR
DRIVE

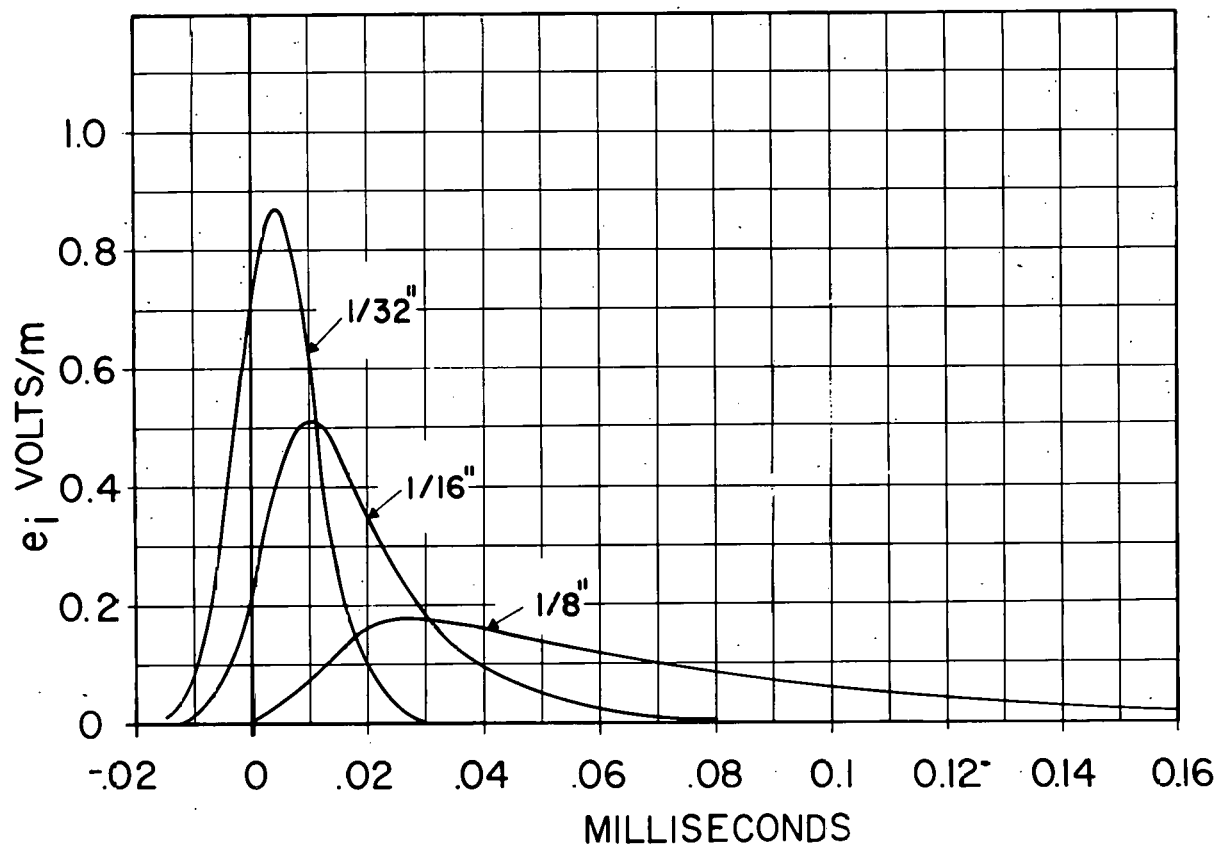
$$\lambda_o = 2.61b$$

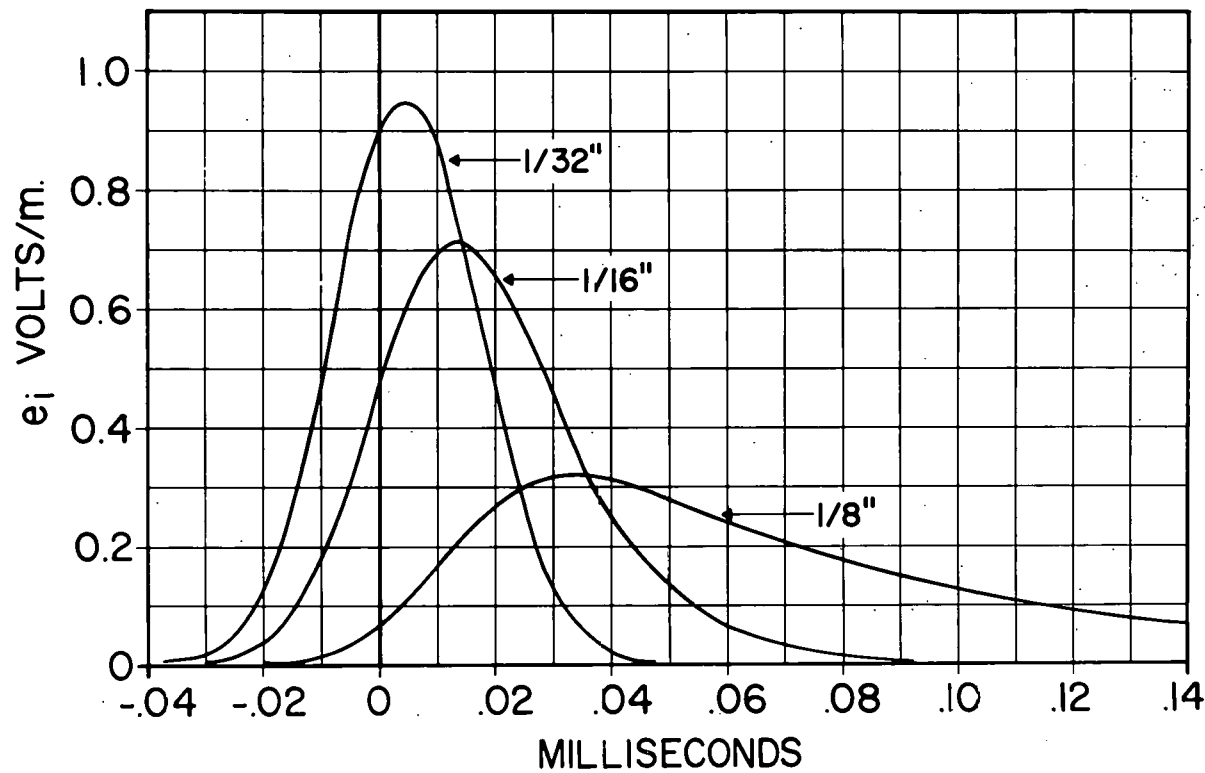
Figure 1 -- Configurations considered in the propagation of gaussian pulses through aluminum walls

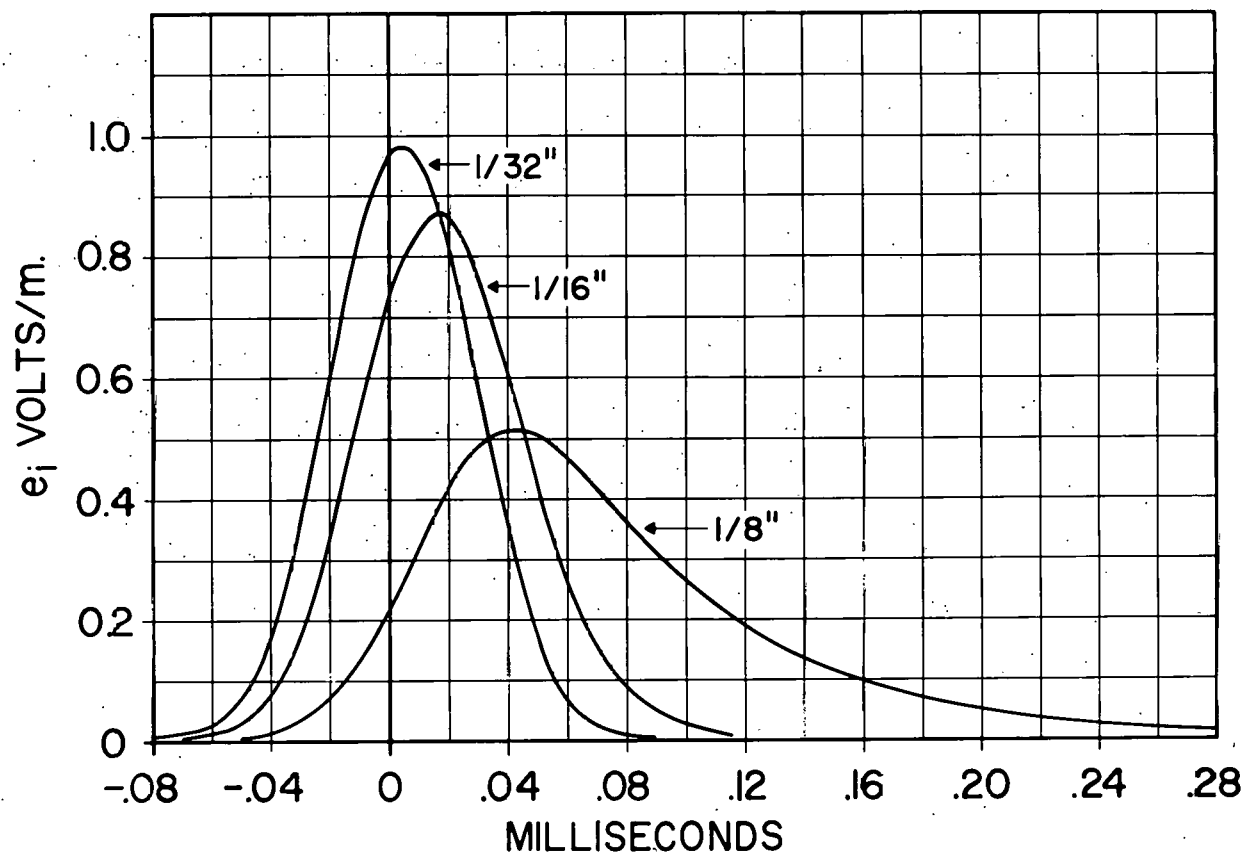


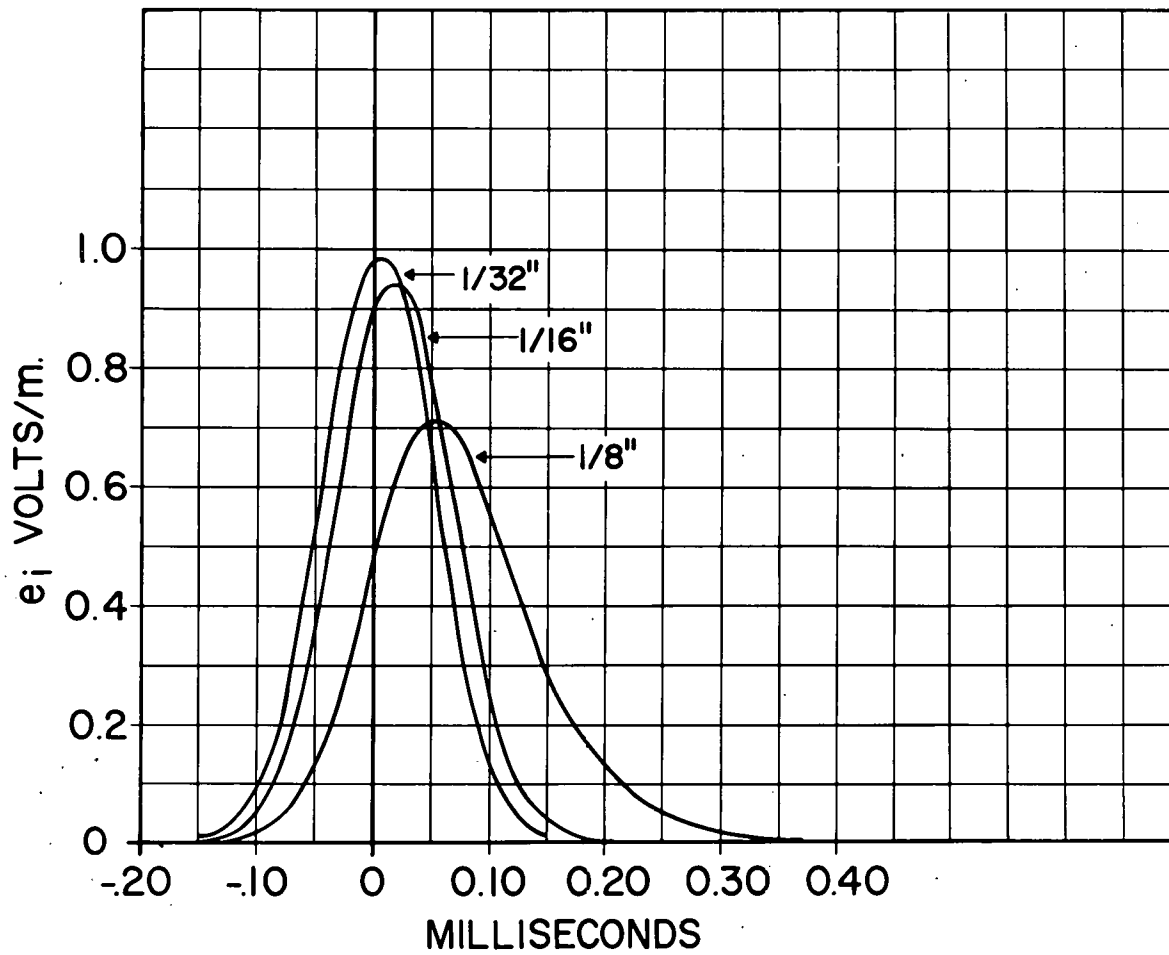
Graph 1 -- Input gaussian pulses

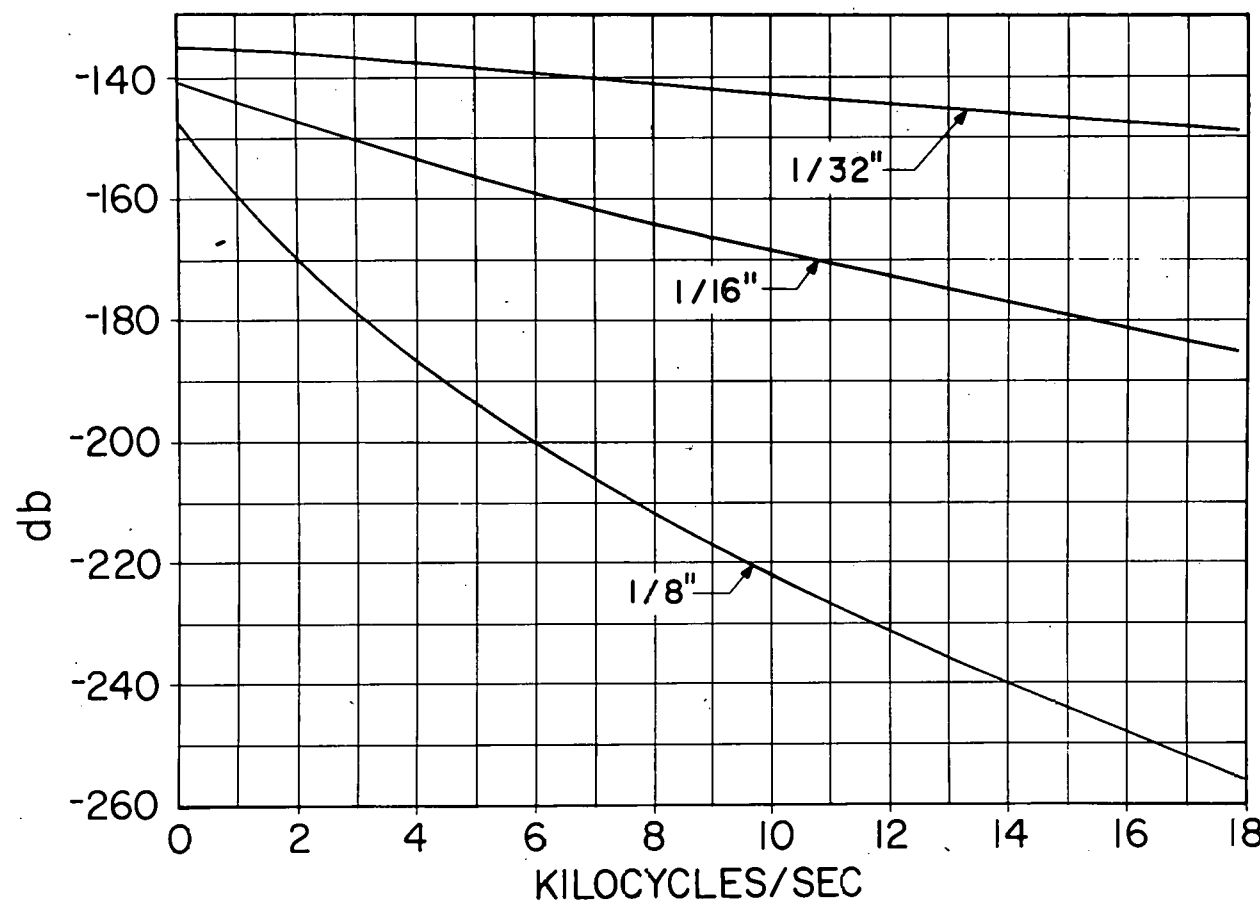


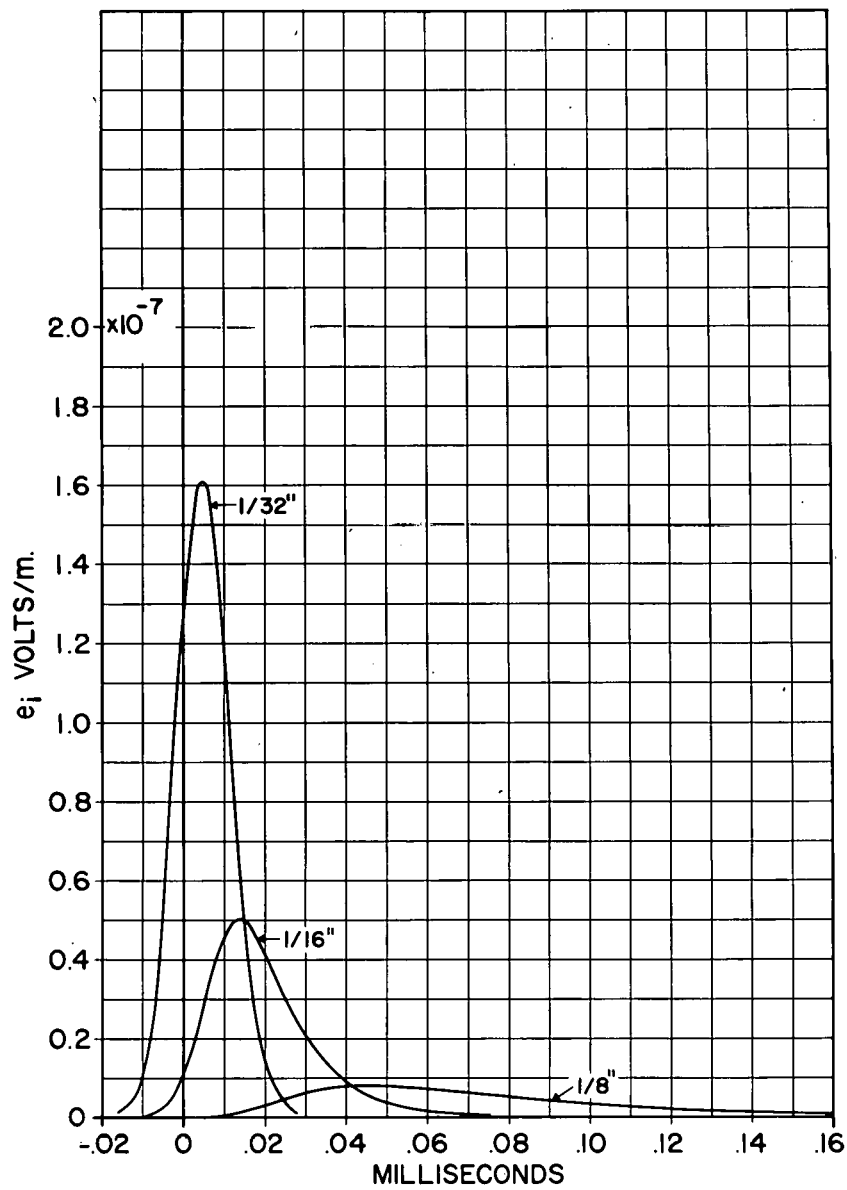


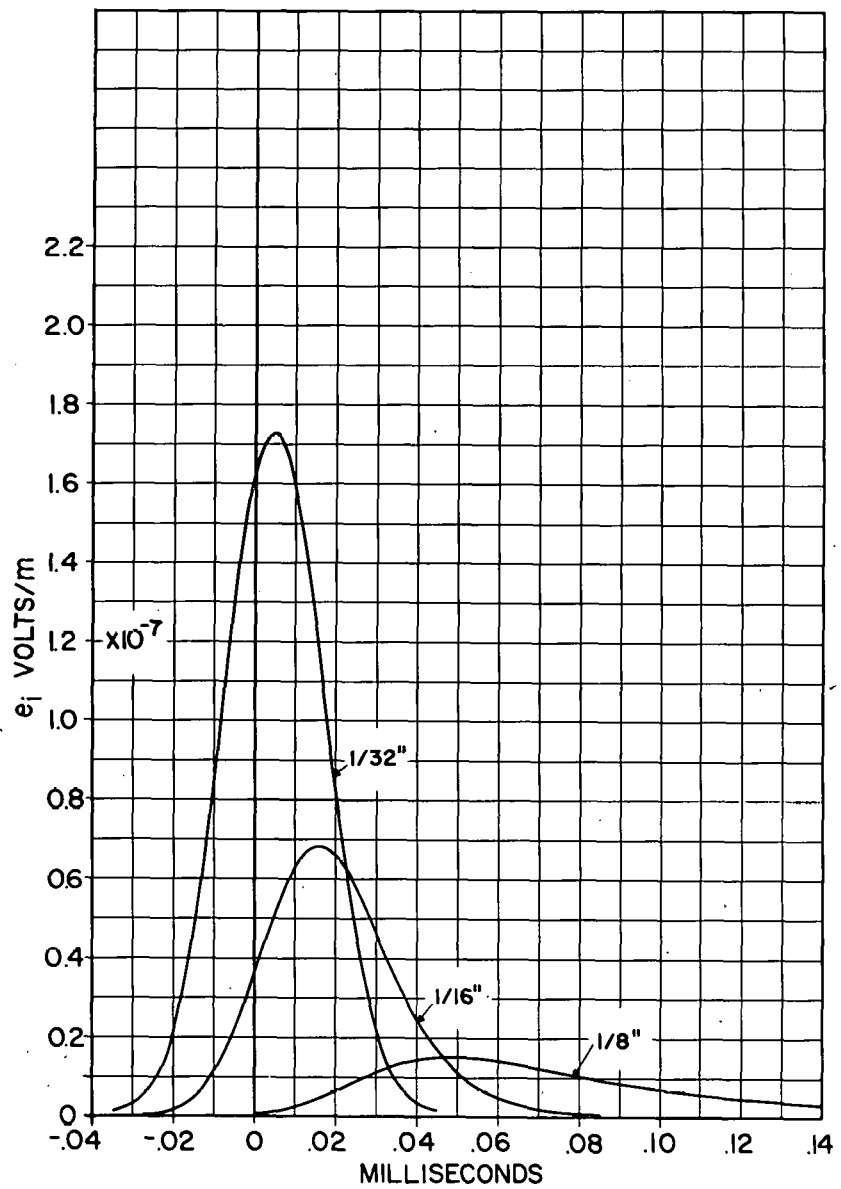


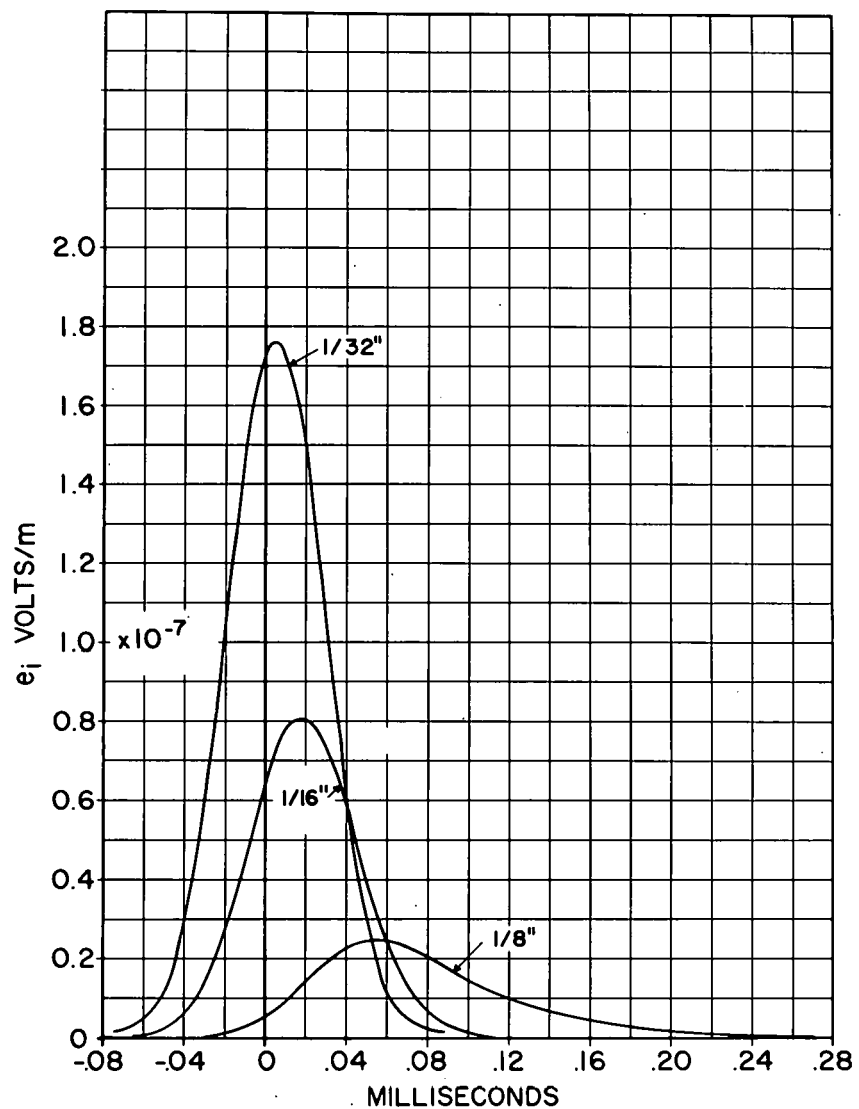




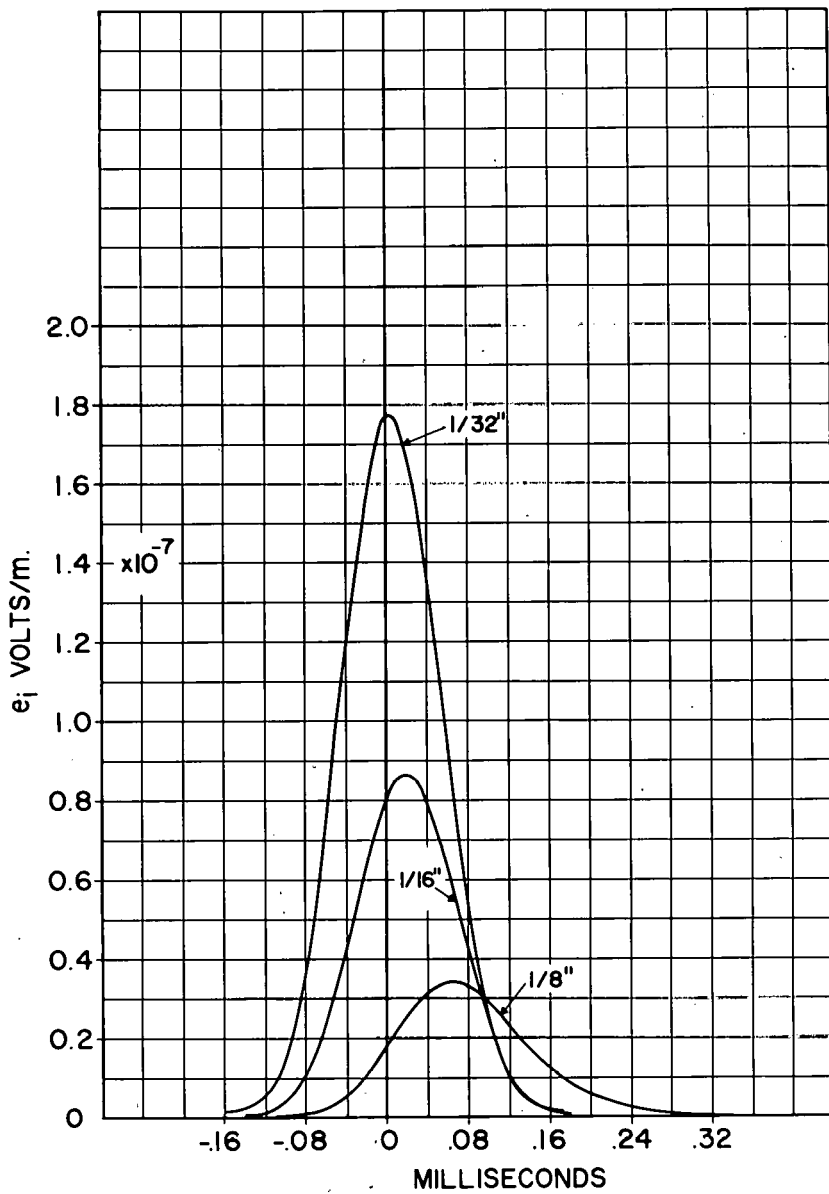


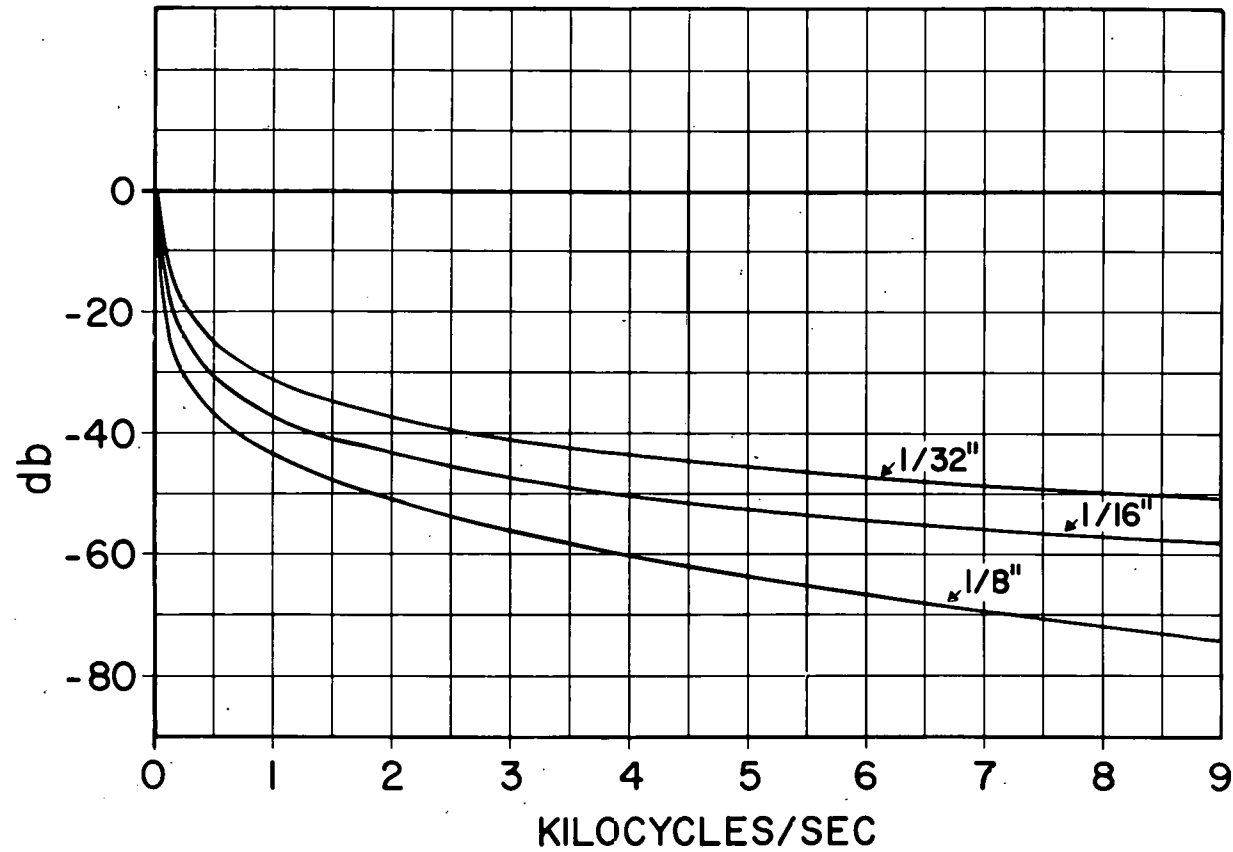


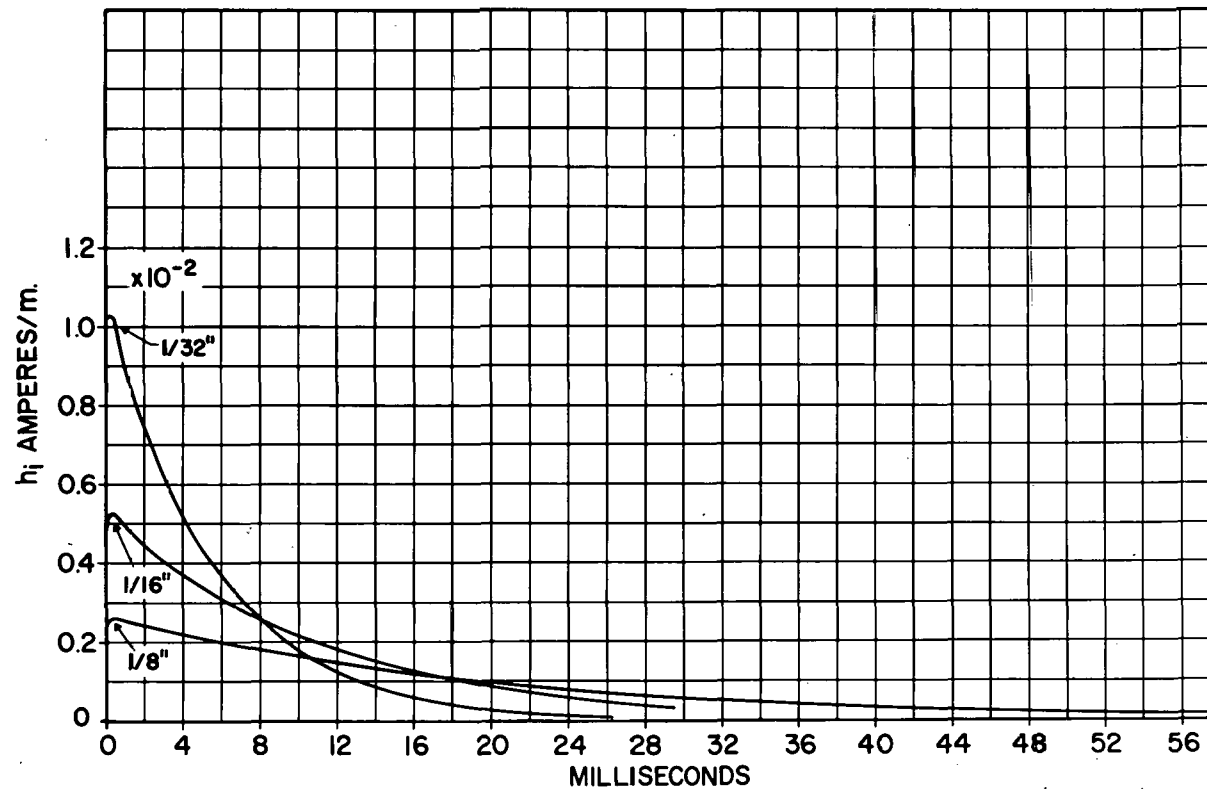


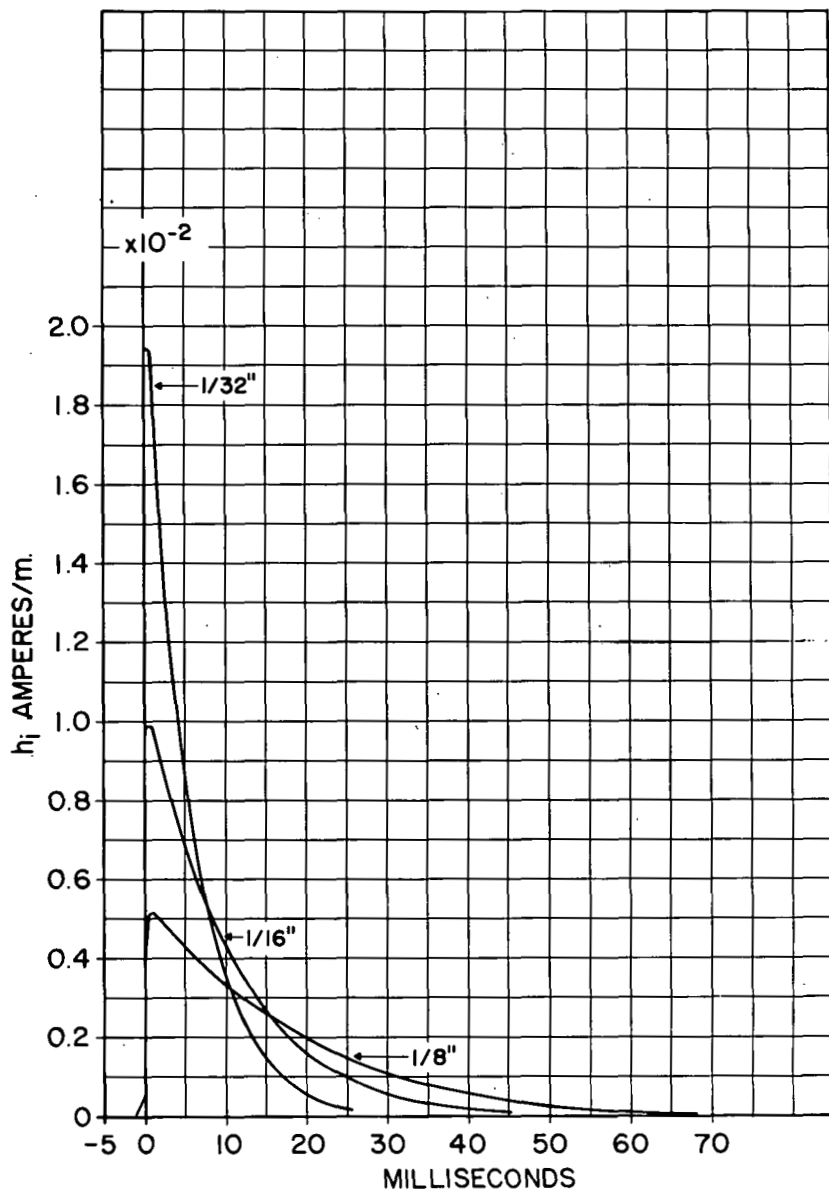


Graph 10 -- Infinite plate. $e_o(0) = 1$ volt/m; $t_1 = 24 \mu s$

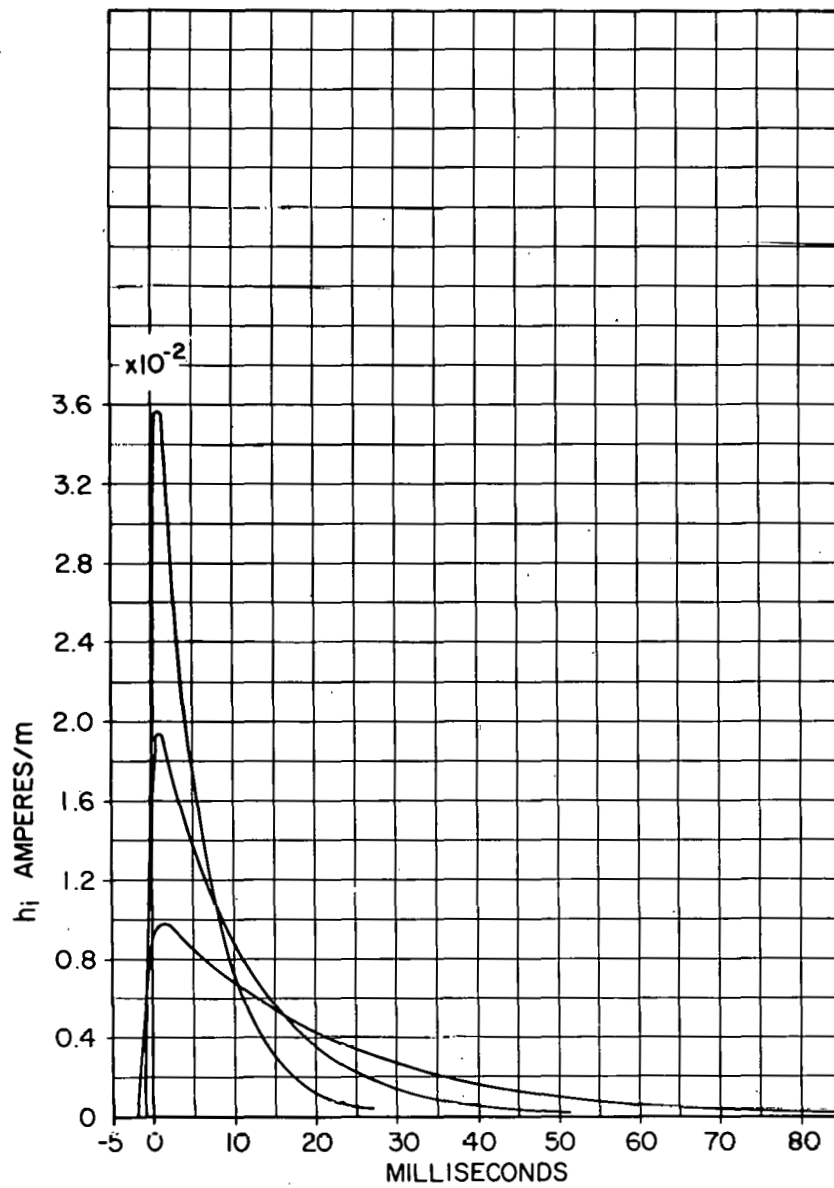




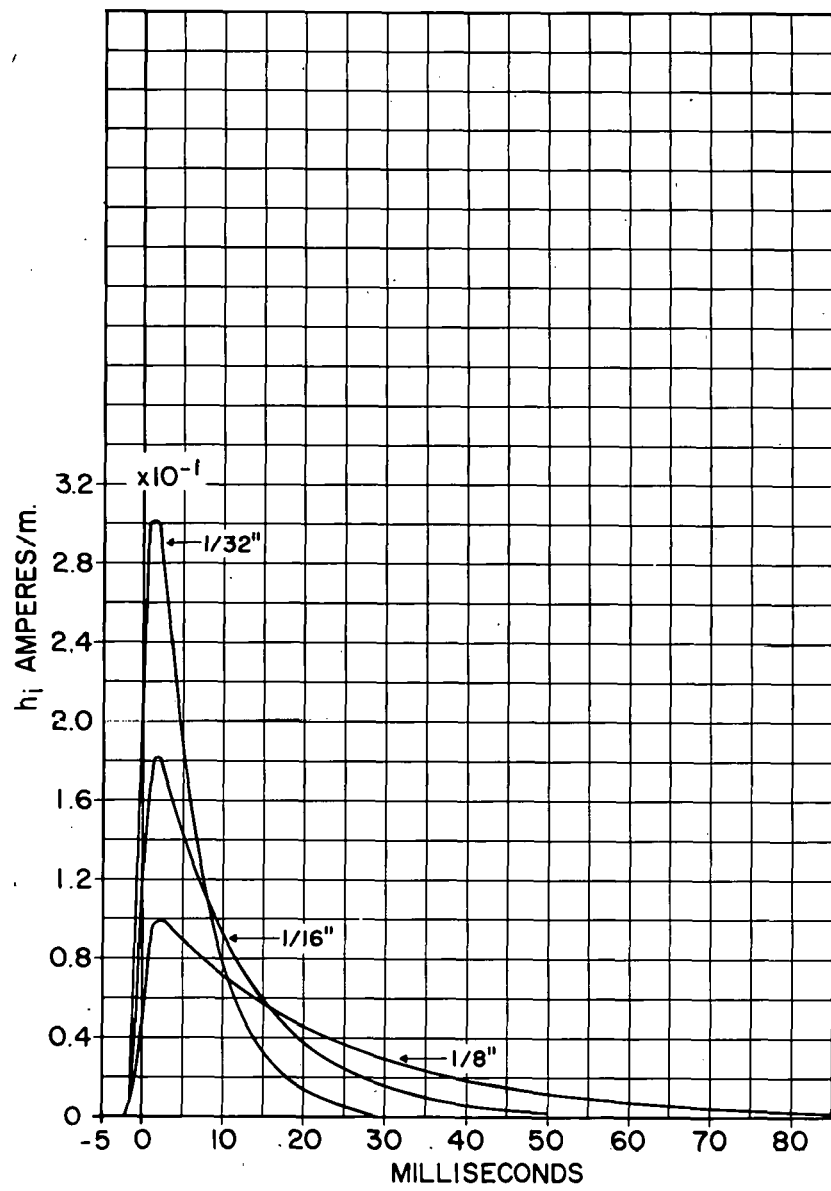




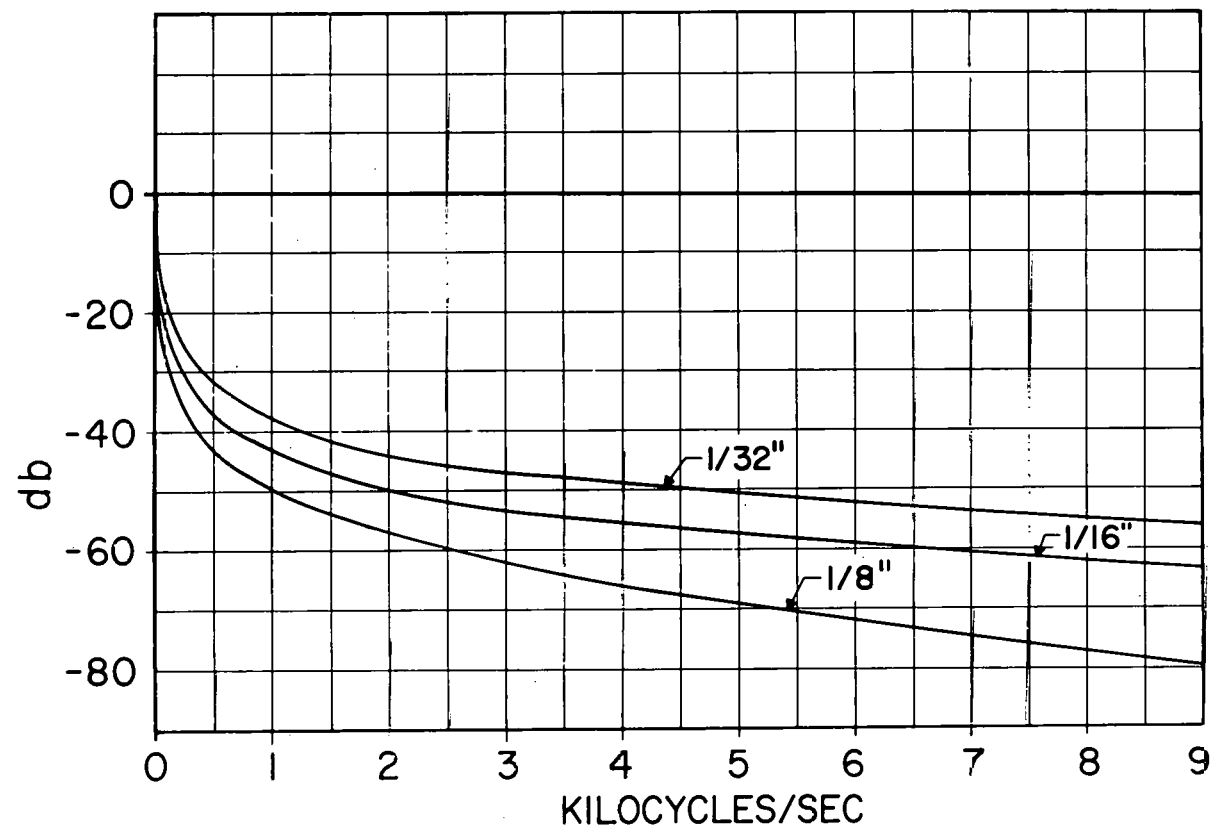
Graph 14 -- Sphere 36 inches in diameter. $h_i(0) = 1$ ampere/m; $t_1 = 48 \mu\text{s}$



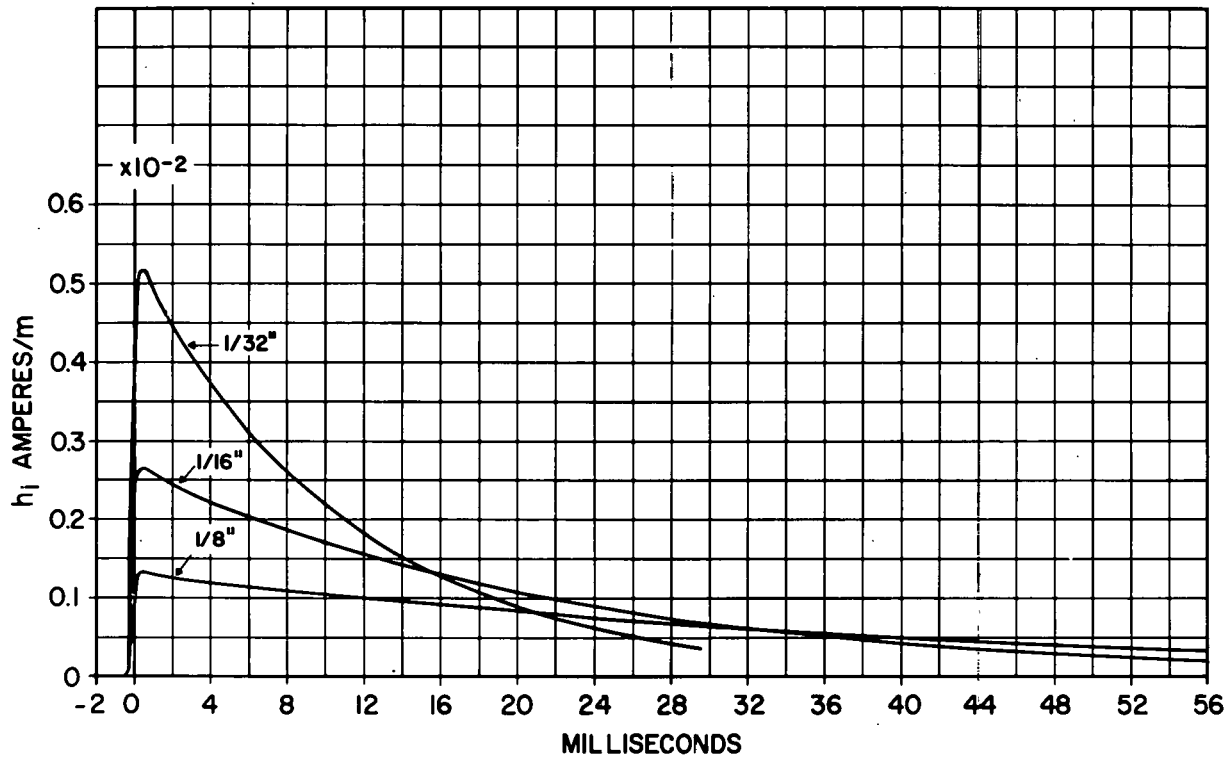
Graph 15 -- Sphere 36 inches in diameter. $h_o(0) = 1$ ampere/m; $t_1 = 96 \mu\text{s}$

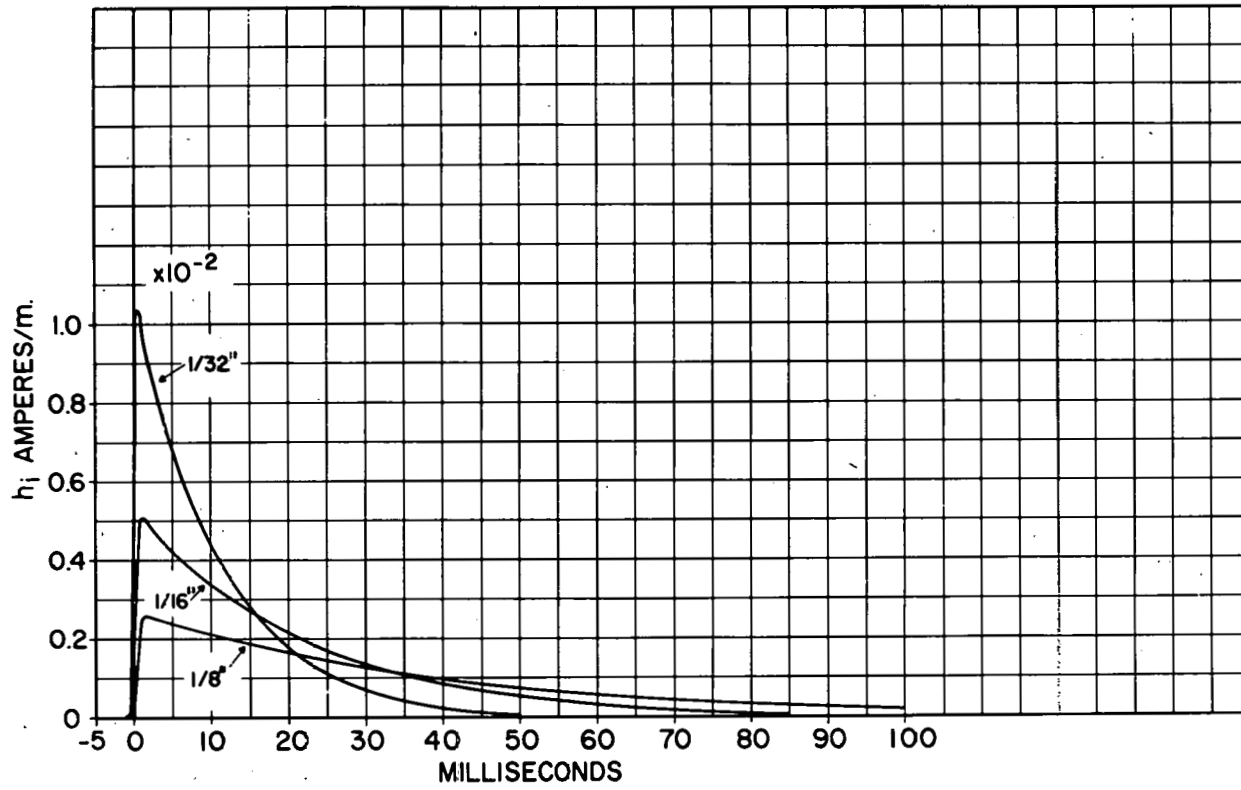


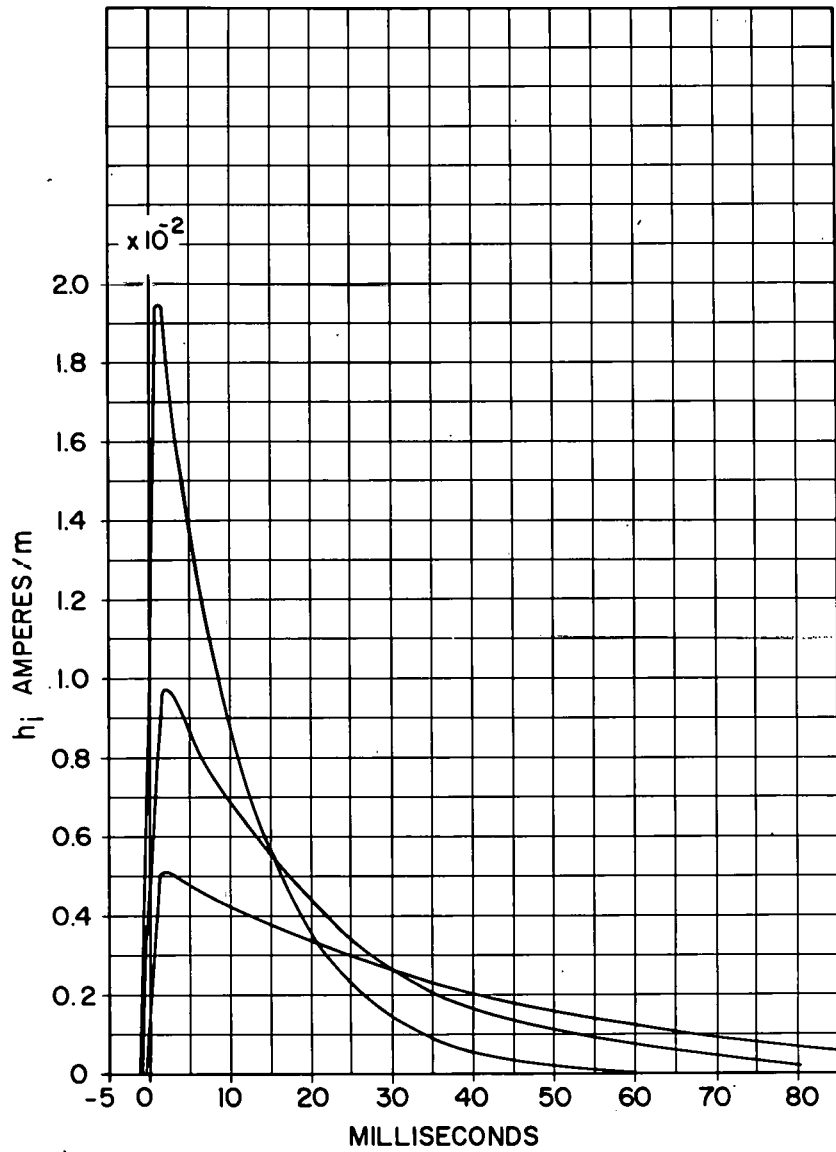
Graph 16 -- Sphere 36 inches in diameter. $h_0(0) = 1$ ampere/m; $t_1 = 1000 \mu s$

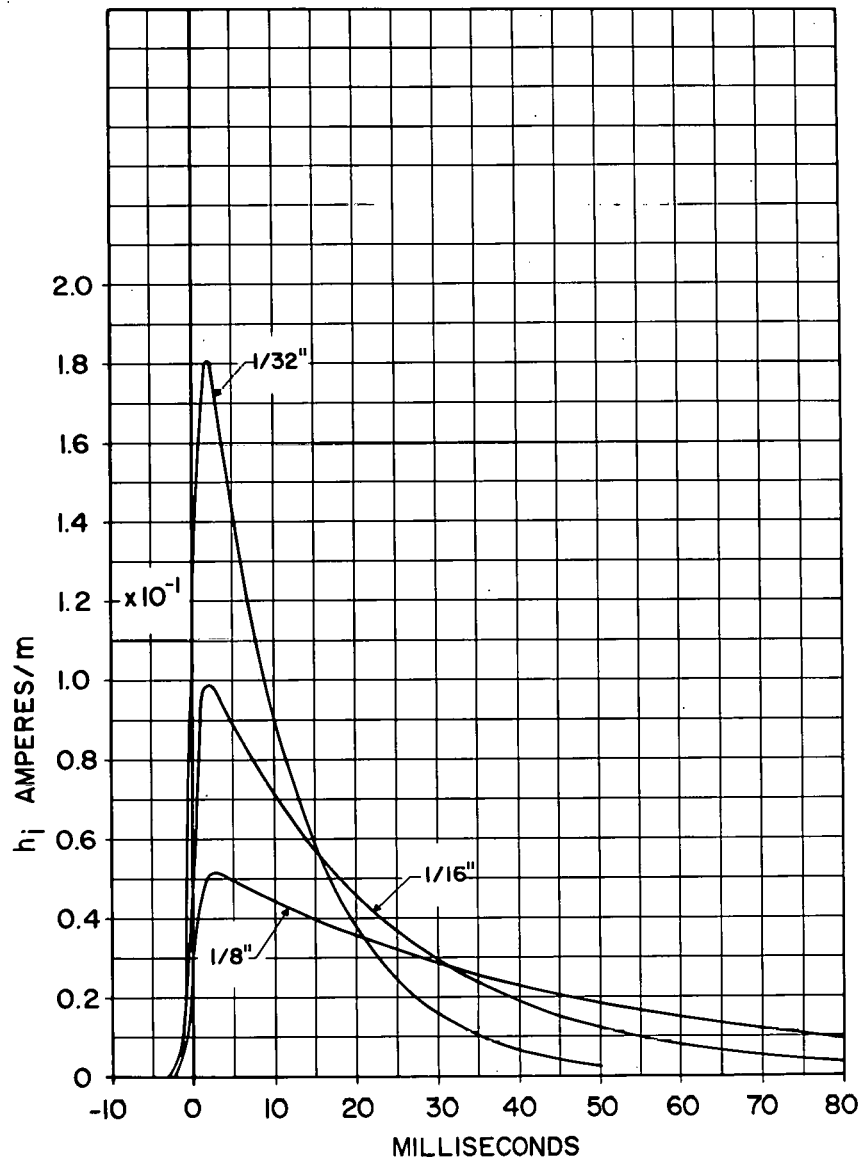


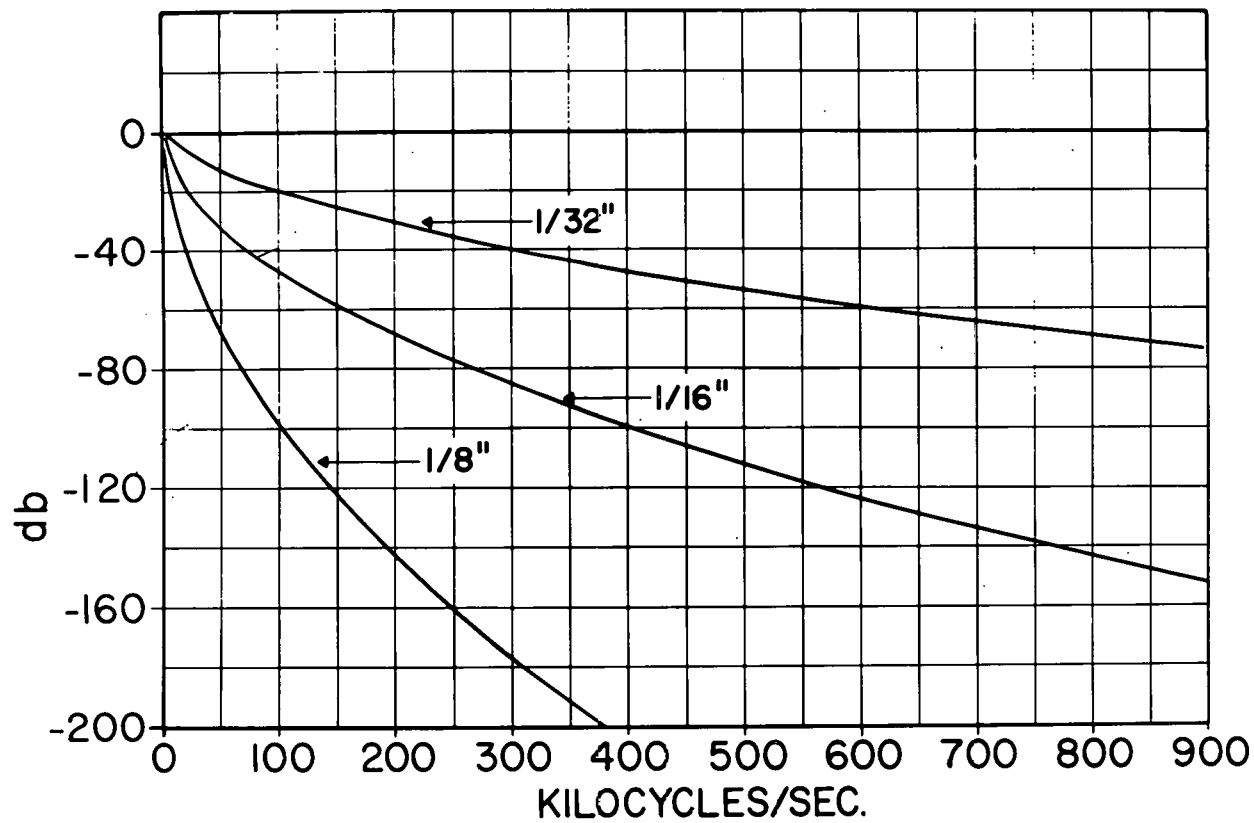
Graph 17 -- Sphere 72 inches in diameter. Steady-state transfer characteristic relating H_i to H_o



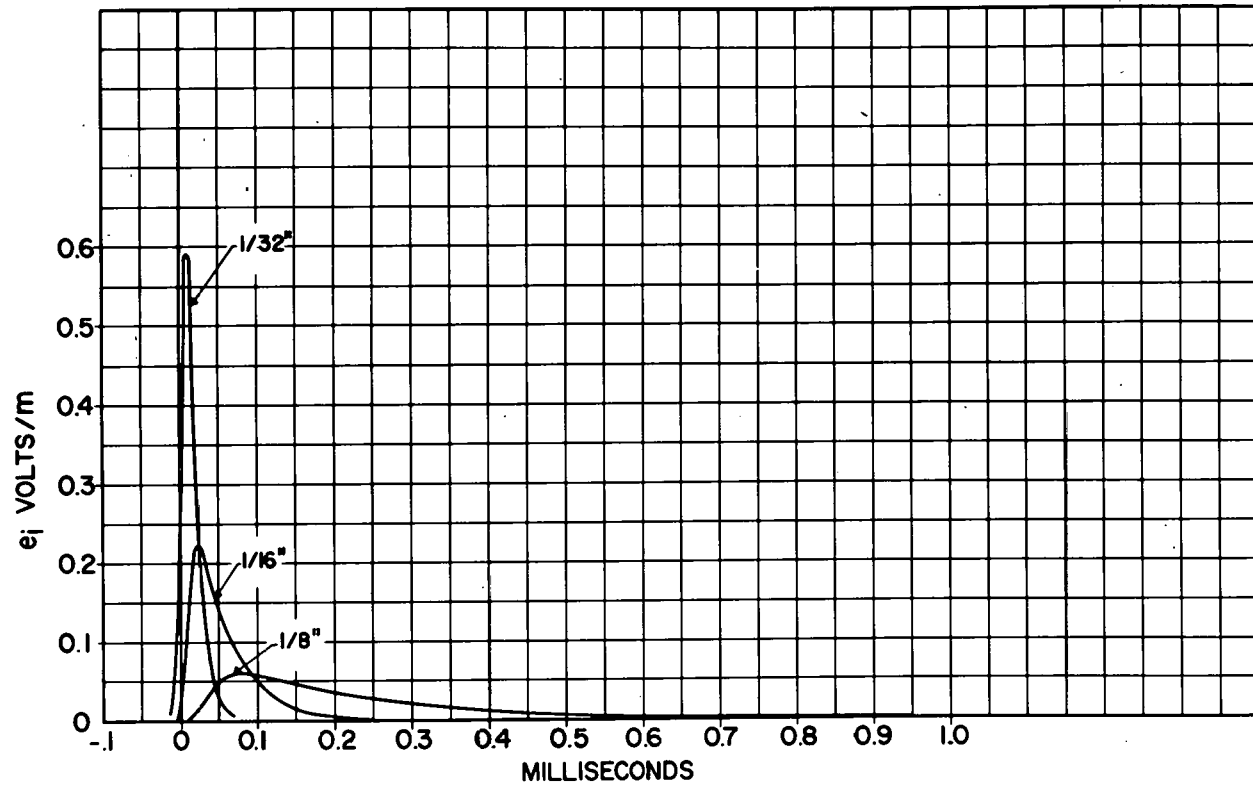


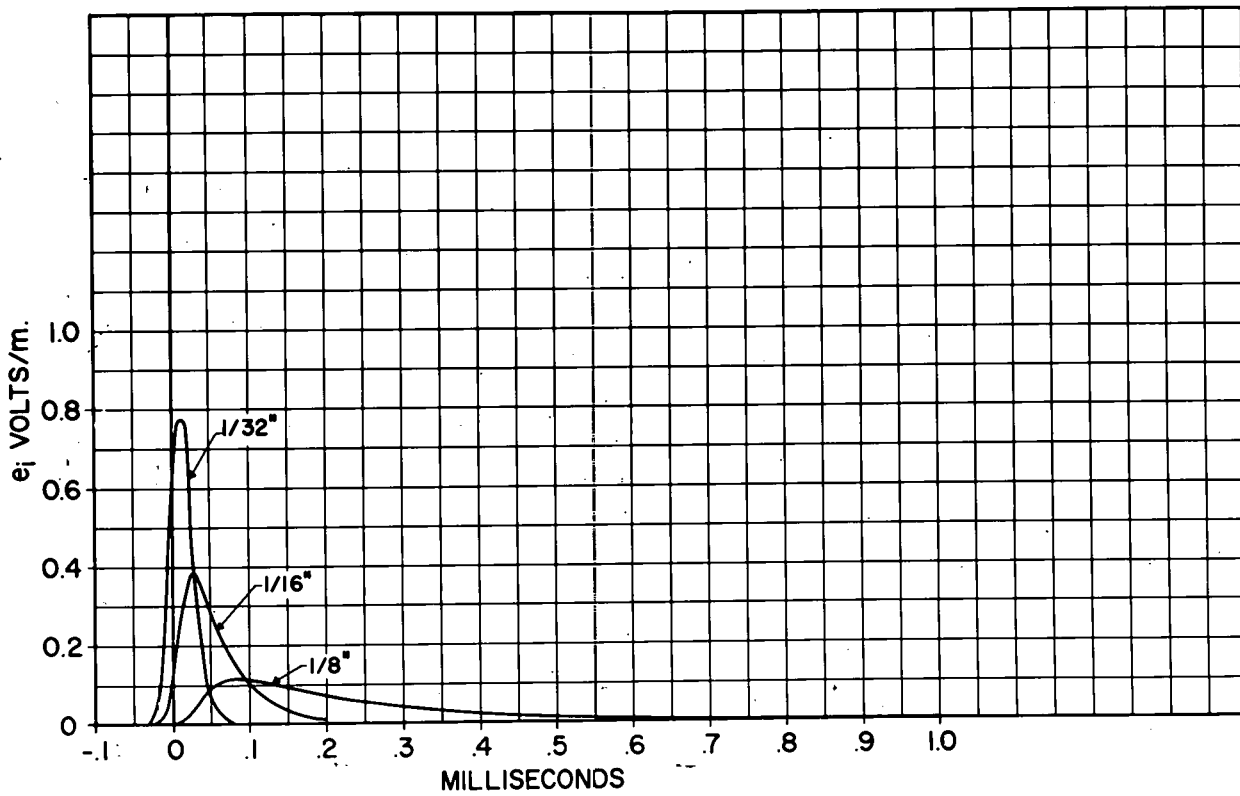


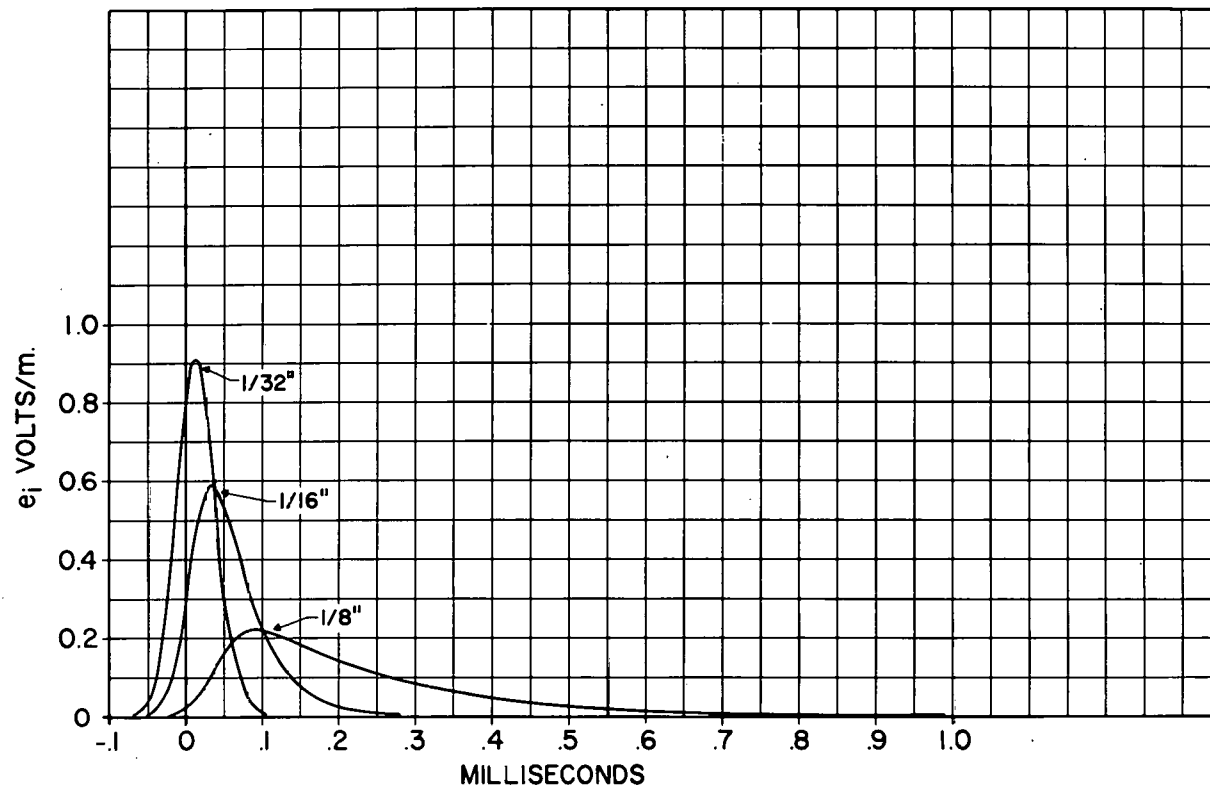


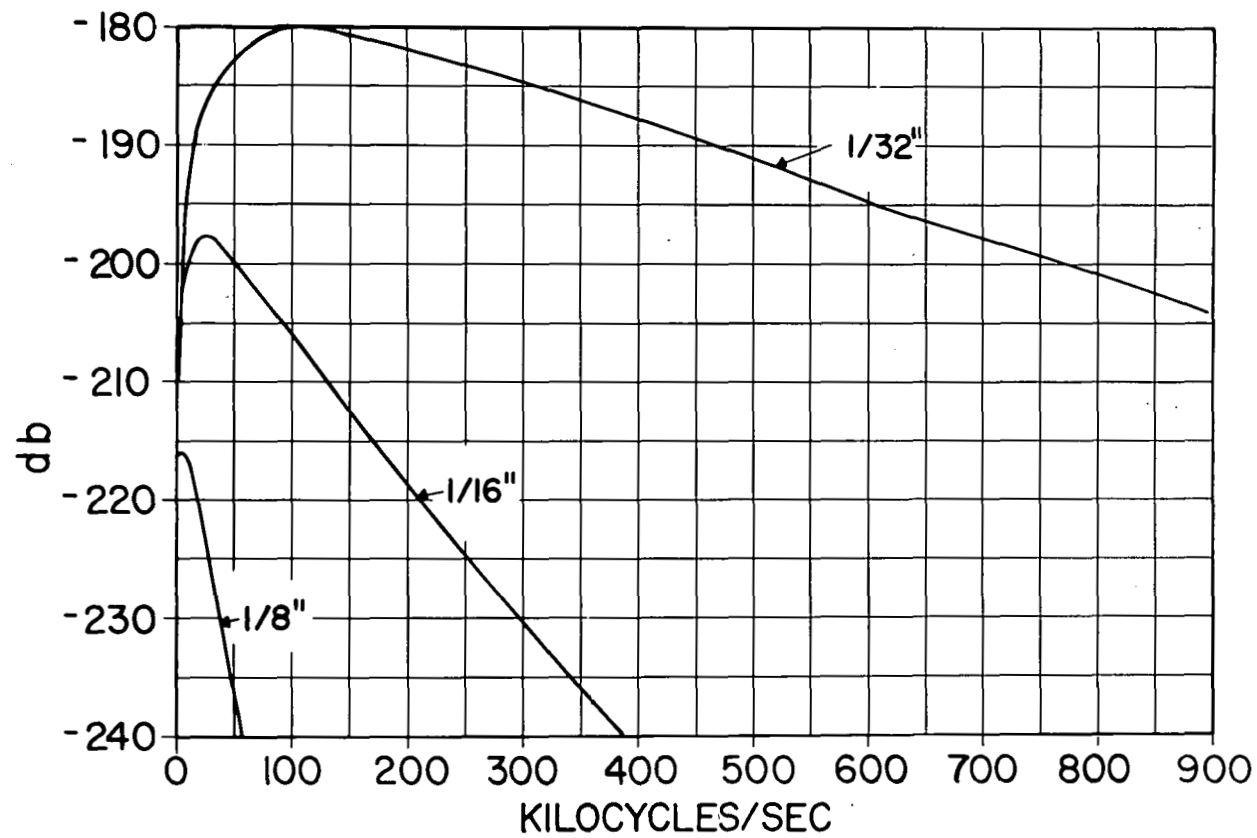


Graph 22 -- Cylinder. Steady-state transfer characteristic relating E_i to E_t

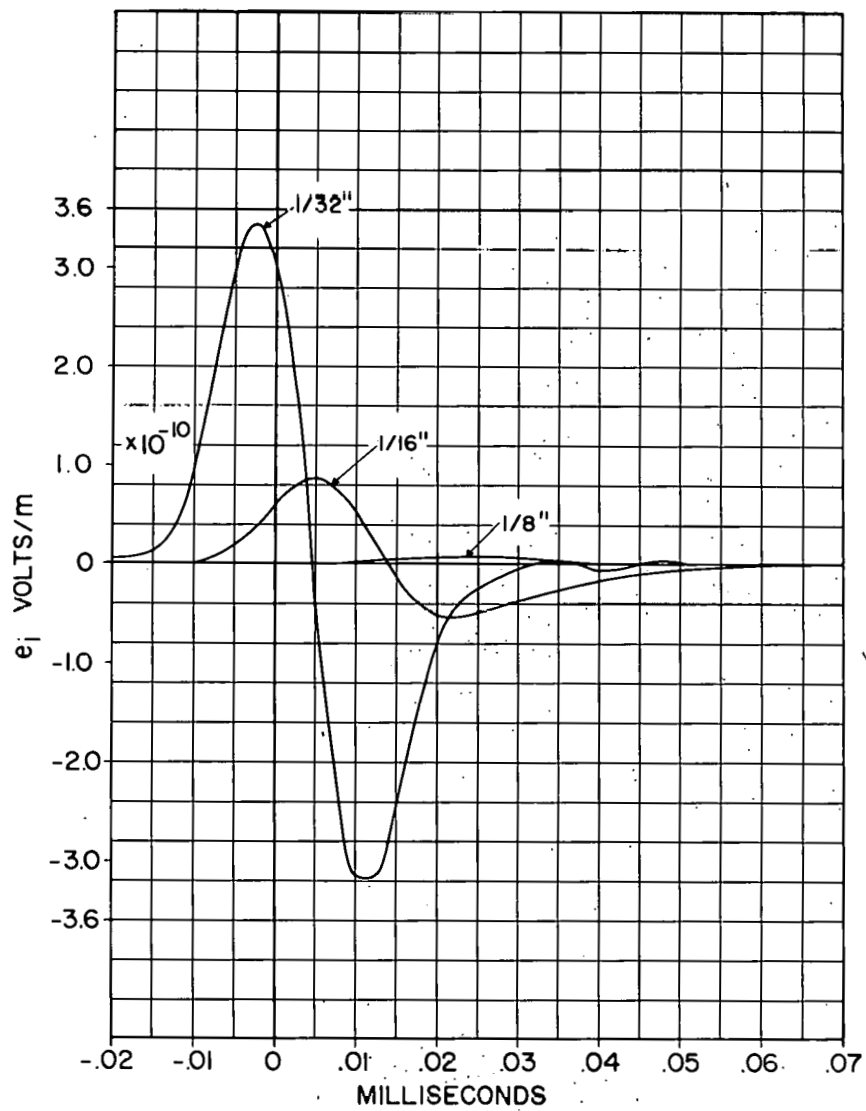


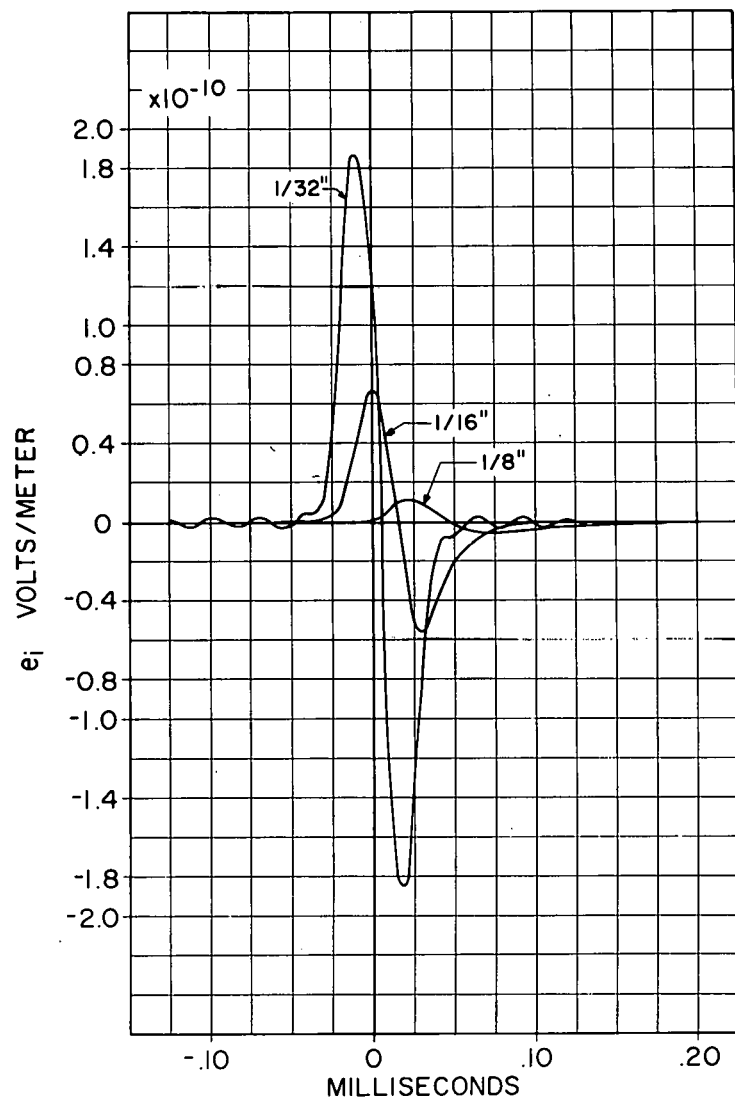




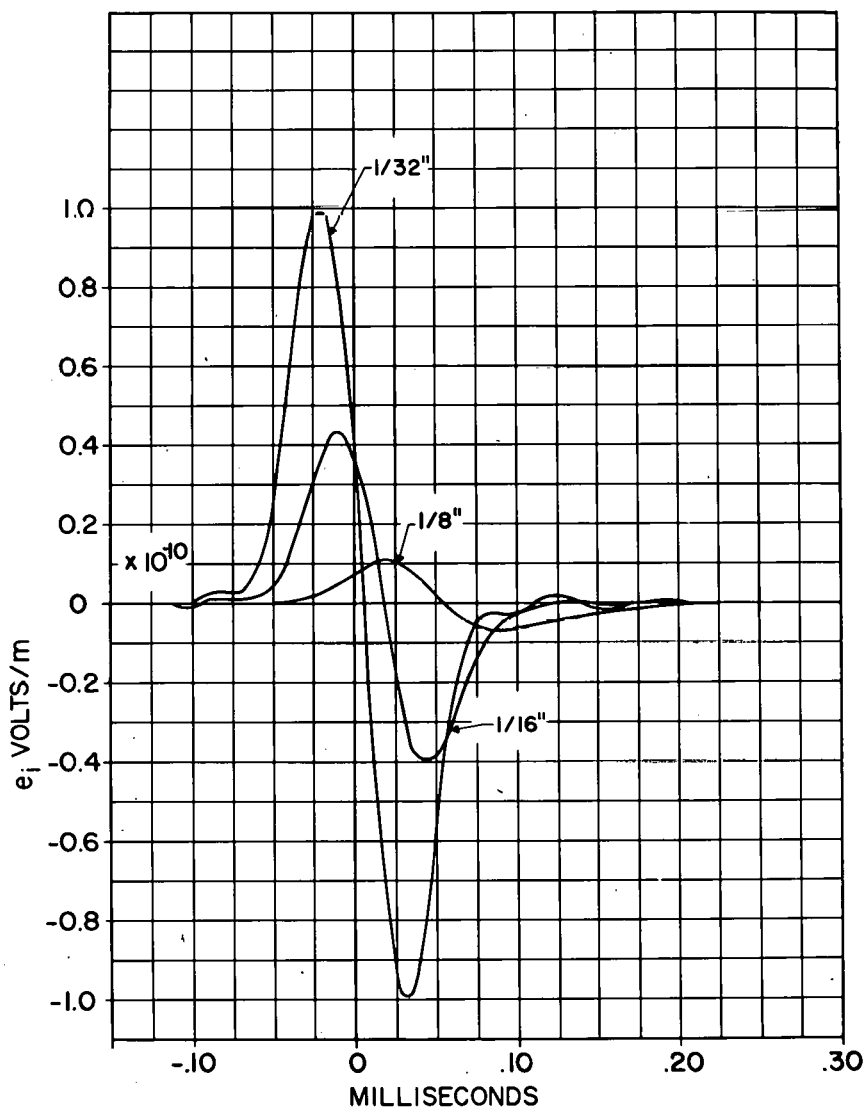


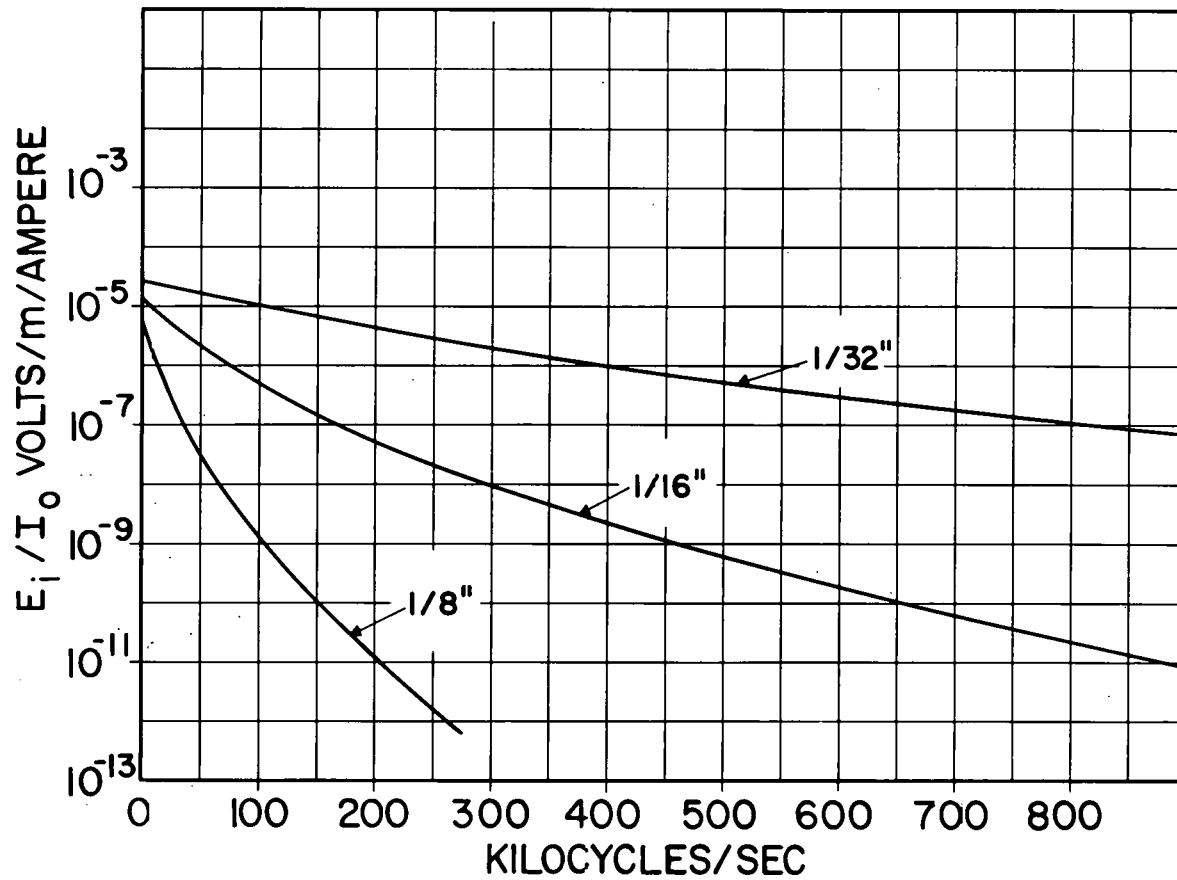
Graph 26 -- Cylinder. Steady-state transfer characteristic relating E_i to E_o



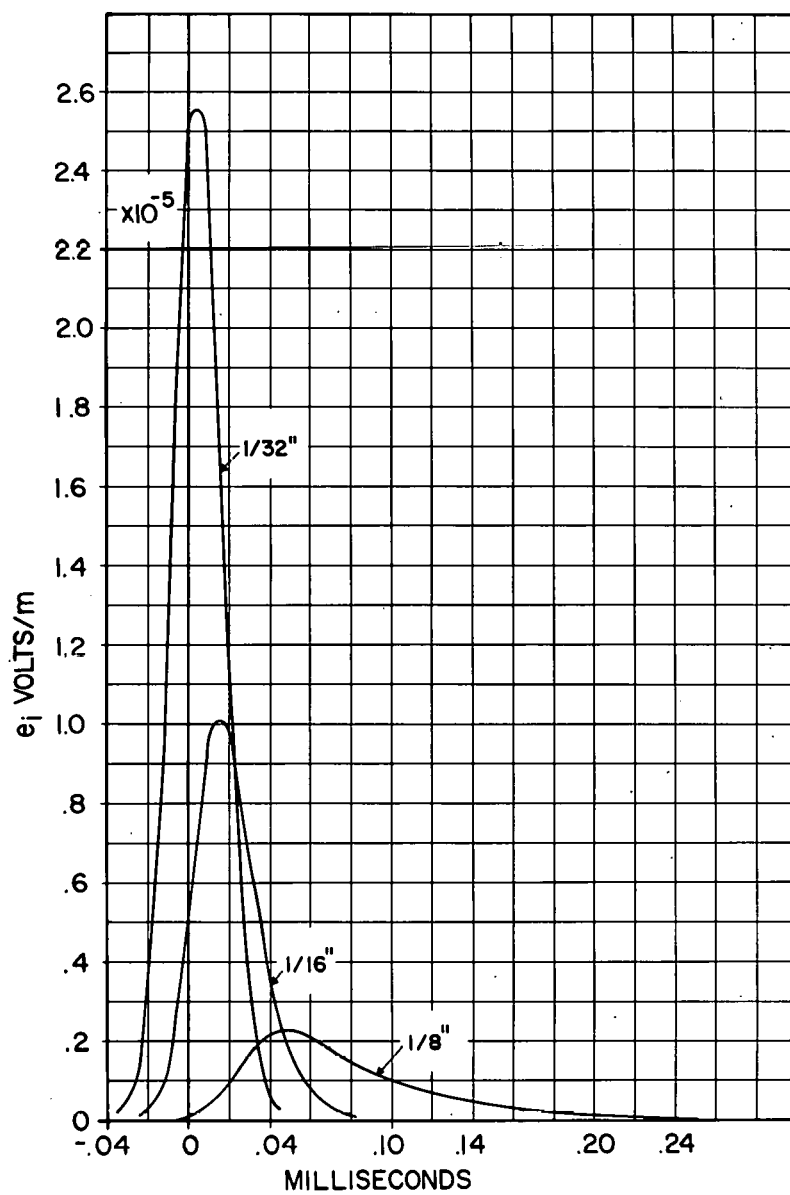


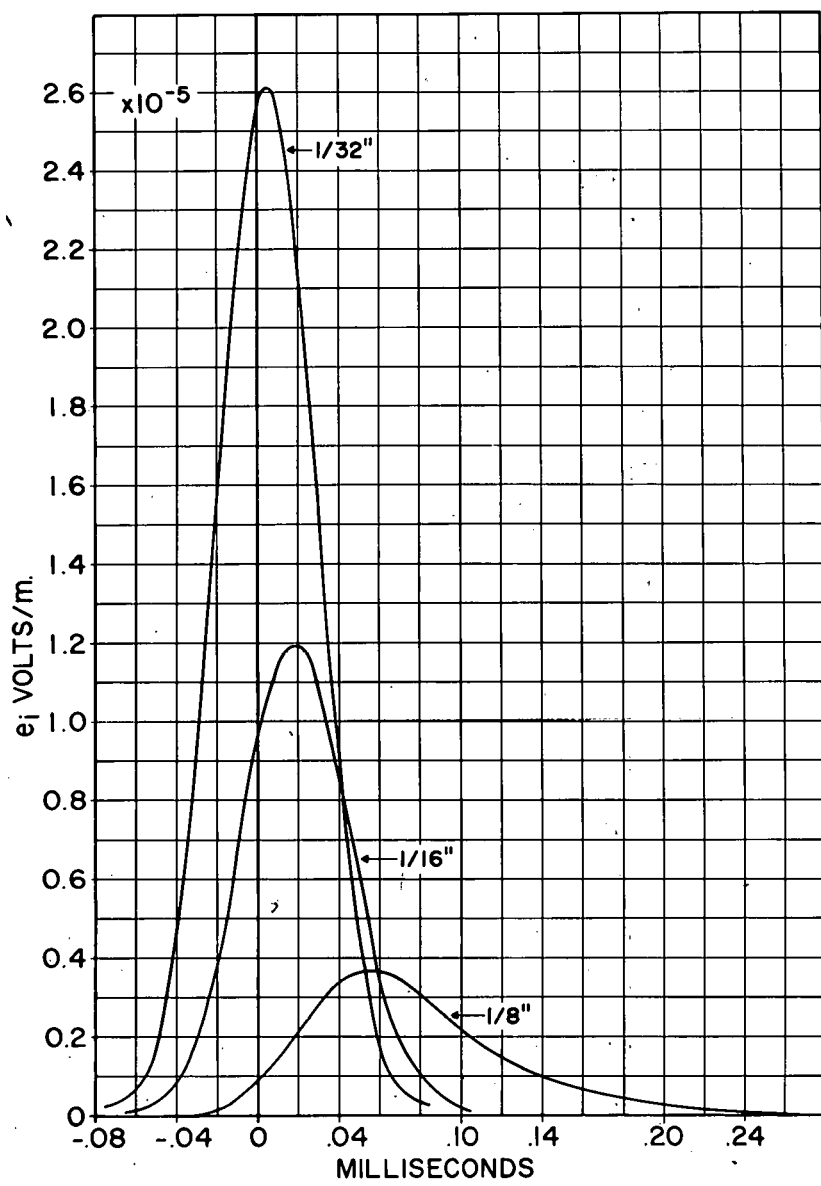
Graph 28 -- Cylinder. $e_o(0) = 1 \text{ volt/m}$; $t_1 = 12 \mu\text{s}$



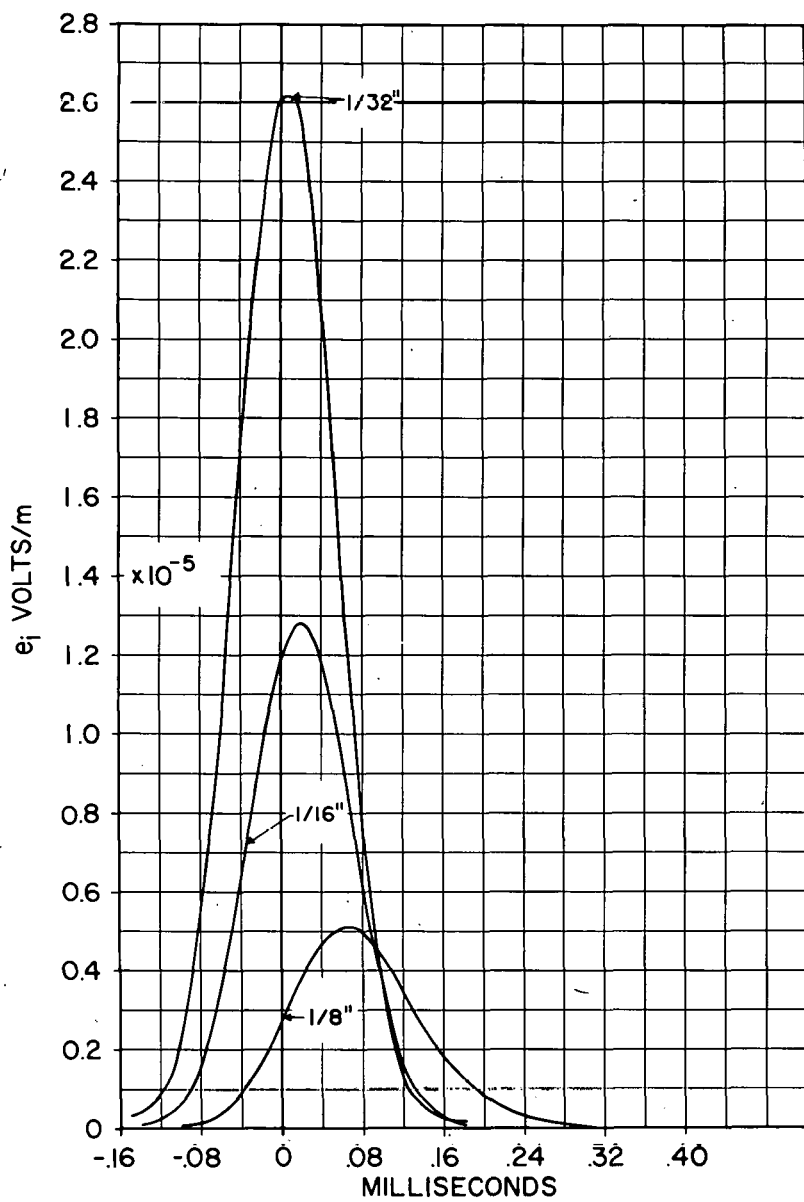


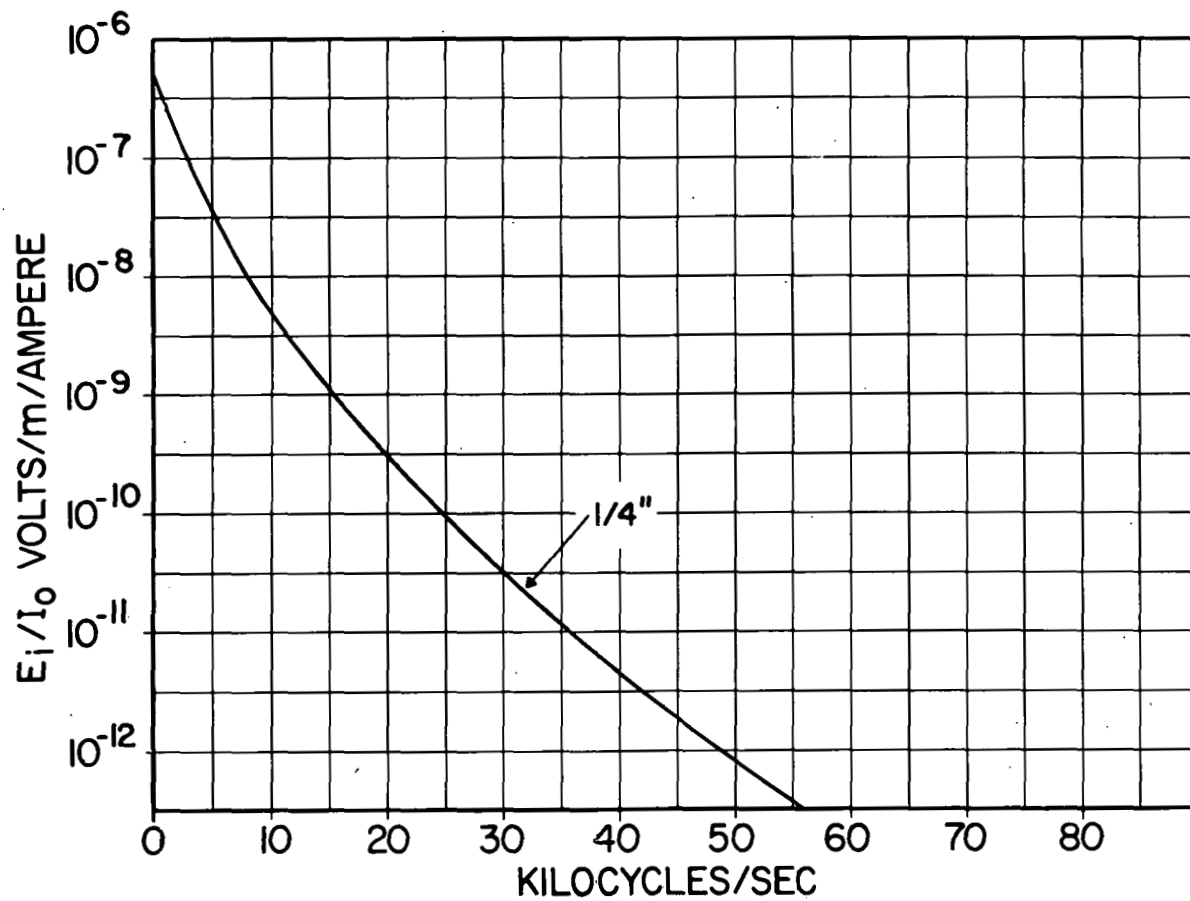
Graph 30 -- Cylinder. Steady-state transfer characteristic relating E_i to I_o .



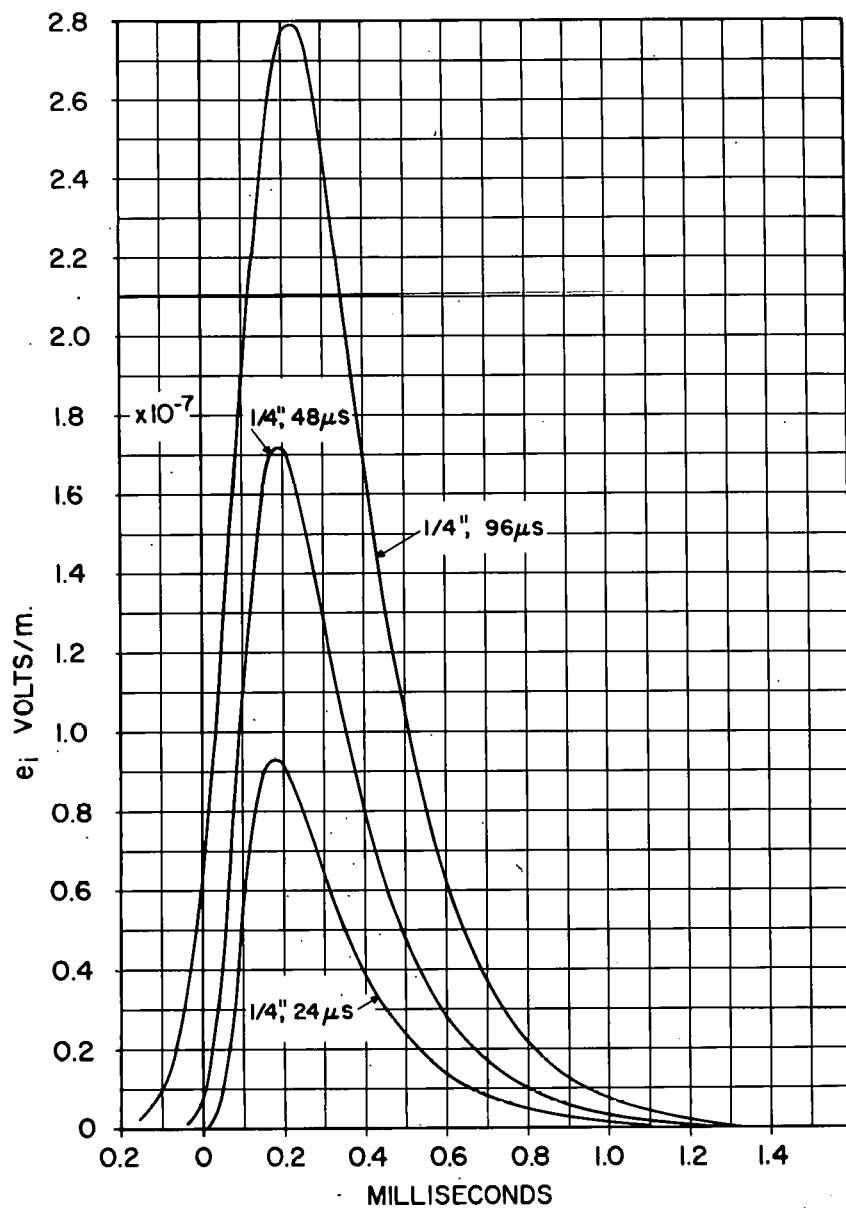


Graph 32 -- Cylinder. $i_o(0) = 1$ ampere; $t_1 = 24 \mu\text{s}$





Graph 34 -- Jupiter missile. Steady-state transfer characteristic relating E_i to I_o



Graph 35 -- Jupiter missile. $i_o(0) = 1$ ampere; $t_1 = 24, 48, \text{ and } 96 \mu\text{s}$

REFERENCES

1. Stratton, J. A., Electromagnetic Theory, McGraw-Hill Book Co., Inc., (1941), Chapter 9, Section 9.10, pp 511-513.
2. Kinsler, L. E. and Frey, A. R., Fundamentals of Acoustics, John Wiley and Sons, Inc., (1950), Chapter 6, Section 6.4, pp 149-154.
3. King, L. V., "Electromagnetic Shielding at Radio Frequencies," Philosophical Magazine and Journal of Science, Vol. 15, No. 97, pp 201-223, February 1933. There appear to be a number of inconsistencies in this paper. If the time dependence is taken to be $\exp(j2\pi ft)$ King's formula (25) reproduced in this paper as (12) appears to be correct, provided $\kappa = \gamma = \sqrt{\pi f \mu \sigma} (1 + j)$.
4. Harrison, C. W. Jr., and King, R. W. P., "Response of a Loaded Electric Dipole in an Imperfectly Conducting Cylinder of Finite Length," Journal of Research of the National Bureau of Standards - D. Radio Propagation, Vol. 64D, No. 3, Equations (15) and (26).
5. McLachan, N. W., Bessel Functions for Engineers, Oxford University Press, 1955 2nd Edition p 32.
6. King, R. W. P., Theory of Linear Antennas, Harvard University Press (1956), Chapter 2, Section 31, p 184, Equations (4a) and (4b), and Chapter 4, Section 9, p 487, Equation (21).

SUPPLEMENTAL REFERENCES

Anderson, W. L., and Moore, R. K., "Frequency Spectra of Transient Electromagnetic Pulses in a Conducting Medium," IRE Transactions on Antennas and Propagation, AP-8, pp 603-607, November 1960.

Richards, P. I., "Transients in Conducting Media," IRE Transactions on Antennas and Propagation, AP-6, pp 178-182, April 1958.

Wait, J. R., "Shielding of a Transient Electromagnetic Dipole Field by a Conductive Sheet," Canadian Journal of Physics, 34, pp 890-893, 1956.

Wait, J. R., "Induction in a Conducting Sheet by a Small Current Carrying Loop," Applied Science Research B3, p 230, 1953.

Zisk, S. H., "Electromagnetic Transients in Conducting Media," IRE Transactions on Antennas and Propagation, AP-8, pp 229-230, March 1960.

Zitron, N. R., "Shielding of Transient Electromagnetic Signals by a Thin Conducting Sheet," Journal of Research of the NBS - D. Radio Propagation, 64D, No. 5, pp 563-567, September-October 1960.